The Cryosphere Discuss., 9, 4147–4203, 2015
www.the-cryosphere-discuss.net/9/4147/2015/
doi:10.5194/tcd-9-4147-2015

The Cryosphere Discussions
Open Access

Numerical simulations of the Cordilleran ice sheet through the last glacial cycle

J. Seguinot[1,2,3], I. Rogozhina[3], A. P. Stroeven[2], M. Margold[2], and J. Kleman[2]

[1]Laboratory of Hydraulics, Hydrology and Glaciology, ETH Zürich, Zürich, Switzerland
[2]Department of Physical Geography and the Bolin Centre for Climate Research, Stockholm University, Stockholm, Sweden
[3]Helmholtz Centre Potsdam, GFZ German Research Centre for Geosciences, Potsdam, Germany

Received: 21 June 2015 – Accepted: 25 June 2015 – Published: 7 August 2015

Correspondence to: J. Seguinot (seguinot@vaw.baug.ethz.ch)

Published by Copernicus Publications on behalf of the European Geosciences Union.

Abstract

Despite more than a century of geological observations, the Cordilleran ice sheet of North America remains poorly understood in terms of its former extent, volume and dynamics. Although geomorphological evidence is abundant, its complexity is such that whole ice-sheet reconstructions of advance and retreat patterns are lacking. Here we use a numerical ice sheet model calibrated against field-based evidence to attempt a quantitative reconstruction of the Cordilleran ice sheet history through the last glacial cycle. A series of simulations is driven by time-dependent temperature offsets from six proxy records located around the globe. Although this approach reveals large variations in model response to evolving climate forcing, all simulations produce two major glaciations during marine oxygen isotope stages 4 (61.9–56.5 ka) and 2 (23.2–16.8 ka). The timing of glaciation is better reproduced using temperature reconstructions from Greenland and Antarctic ice cores than from regional oceanic sediment cores. During most of the last glacial cycle, the modelled ice cover is discontinuous and restricted to high mountain areas. However, widespread precipitation over the Skeena Mountains favours the persistence of a central ice dome throughout the glacial cycle. It acts as a nucleation centre before the Last Glacial Maximum and hosts the last remains of Cordilleran ice until the middle Holocene (6.6–6.2 ka).

1 Introduction

During the last glacial cycle, glaciers and ice caps of the North American Cordillera have been more extensive than today. At the Last Glacial Maximum (LGM), a continuous blanket of ice, the Cordilleran ice sheet (Dawson, 1888), stretched from the Alaska Range in the north to the North Cascades in the south (Fig. 1). In addition, it extended offshore, where it calved into the Pacific Ocean, and merged with the western margin of its much larger neighbour, the Laurentide ice sheet, east of the Rocky Mountains.

TCD
9, 4147–4203, 2015

More than a century of exploration and geological investigation of the Cordilleran mountains have led to many observations in support of the former ice sheet (Jackson and Clague, 1991). Despite the lack of documented end moraines offshore, in the zone of confluence with the Laurentide ice sheet, and in areas swept by the Missoula floods (Carrara et al., 1996), moraines that demarcate the northern and southwestern margins provide key constraints that allow reasonable reconstructions of maximum ice sheet extents (Prest et al., 1968; Clague, 1989, Fig. 1.12; Duk-Rodkin, 1999; Booth et al., 2003; Dyke, 2004). As indicated by field evidence from radiocarbon dating (Clague et al., 1980; Clague, 1985, 1986; Porter and Swanson, 1998; Menounos et al., 2008), cosmogenic exposure dating (Stroeven et al., 2010, 2014; Margold et al., 2014), bedrock deformation in response to former ice loads (Clague and James, 2002; Clague et al., 2005), and offshore sedimentary records (Cosma et al., 2008; Davies et al., 2011), the LGM Cordilleran ice sheet extent was short-lived. However, former ice thicknesses and, therefore, the ice sheet's contribution to the LGM sea level lowstand (Carlson and Clark, 2012; Clark and Mix, 2002) remain uncertain.

Our understanding of the Cordilleran glaciation history prior to the LGM is even more fragmentary (Barendregt and Irving, 1998; Kleman et al., 2010; Rutter et al., 2012), although it is clear that the Pleistocene maximum extent of the Cordilleran ice sheet predates the last glacial cycle (Hidy et al., 2013). In parts of the Yukon Territory and Alaska, and in the Puget Lowland, the distribution of tills (Turner et al., 2013; Troost, 2014) and dated glacial erratics (Ward et al., 2007, 2008; Briner and Kaufman, 2008; Stroeven et al., 2010, 2014) indicate an extensive Marine Oxygen Isotope Stage (MIS) 4 glaciation. Landforms in the interior regions include flow sets that are likely older than the LGM (Kleman et al., 2010, Fig. 2), but their absolute age remains uncertain.

In contrast, evidence for the deglaciation history of the Cordilleran ice sheet since the LGM is considerable, albeit mostly at a regional scale. Geomorphological evidence from south-central British Columbia indicates a rapid deglaciation, including an early emergence of elevated areas while thin, stagnant ice still covered the surrounding lowlands (Fulton, 1967, 1991; Margold et al., 2011, 2013b). This model, although cred-

TCD
9, 4147–4203, 2015

ible, may not apply in all areas of the Cordilleran ice sheet (Margold et al., 2013a). Although solid evidence for late-glacial glacier re-advances have been found in the Coast, Columbia and Rocky mountains (Clague et al., 1997; Friele and Clague, 2002a, b; Kovanen, 2002; Kovanen and Easterbrook, 2002; Lakeman et al., 2008; Menounos et al., 2008), it appears to be sparser than for formerly glaciated regions surrounding the North Atlantic (e.g., Sissons, 1979; Lundqvist, 1987; Ivy-Ochs et al., 1999; Stea et al., 2011). Nevertheless, recent oxygen isotope measurements from Gulf of Alaska sediments reveal a climatic evolution highly correlated to that of Greenland during this period, including a distinct Late Glacial cold reversal between 14.1 and 11.7 ka (Praetorius and Mix, 2014).

In general, the topographic complexity of the North American Cordillera and its effect on glacial history have inhibited the reconstruction of ice sheet-wide glacial advance and retreat patterns such as those available for the Fennoscandian and Laurentide ice sheets (Boulton et al., 2001; Dyke and Prest, 1987; Dyke et al., 2003; Kleman et al., 1997, 2010; Stroeven et al., 2015). Here, we use a numerical ice sheet model (the PISM authors, 2015), calibrated against field-based evidence, to perform a quantitative reconstruction of the Cordilleran ice sheet evolution through the last glacial cycle, and analyse some of the long-standing questions related to its evolution:

- How much ice was locked in the Cordilleran ice sheet during the LGM?
- What was the scale of glaciation prior to the LGM?
- Which were the primary dispersal centres? Do they reflect stable or ephemeral configurations?
- How rapid was the last deglaciation? Did it include Late Glacial standstills or readvances?

Although numerical ice sheet modelling has been established as a useful tool to improve our understanding of the Cordilleran ice sheet (Jackson and Clague, 1991,

TCD
9, 4147–4203, 2015

p. 227; Robert, 1991; Marshall et al., 2000), the ubiquitously mountainous topography of the region has presented two major challenges to its application. First, only recent developments in numerical ice sheet models and underlying scientific computing tools (Bueler and Brown, 2009; Balay et al., 2015) have allowed for high-resolution numerical modelling of glaciers and ice sheets on mountainous terrain over millennial time scales (e.g., Golledge et al., 2012). Second, the complex topography of the North American Cordillera also induces strong geographic variations in temperature and precipitation, thus requiring the use of high-resolution climate forcing fields as an input to an ice sheet model (Seguinot et al., 2014). However, evolving climate conditions over the last glacial cycle are subject to considerable uncertainty and still lie beyond the computational reach of atmosphere circulation models.

Our palaeo-climate forcing therefore includes spatial temperature and precipitation grids derived from a present-day atmospheric reanalysis (Mesinger et al., 2006) that includes the steep precipitation gradients previously identified as necessary to model the LGM extent of the Cordilleran ice sheet in agreement with its geological imprint (Seguinot et al., 2014). To mimic climate evolution through the last glacial cycle, these grids are simply supplemented by lapse-rate corrections and temperature offset time series. The latter are obtained by scaling six different palaeo-temperature reconstructions from proxy records around the globe, including two oxygen isotope records from Greenland ice cores (Dansgaard et al., 1993; Andersen et al., 2004), two oxygen isotope records from Antarctic ice cores (Petit et al., 1999; Jouzel et al., 2007), and two alkenone unsaturation index records from Northwest Pacific ocean sediment cores (Herbert et al., 2001). We then proceed to compare the model output to geological evidence and discuss the timing and extent of glaciation and the patterns of deglaciation, based on which we use the applicability of different records to modelling the history of the Cordilleran ice sheet.

TCD
9, 4147–4203, 2015

2 Model setup

2.1 Overview

The simulations presented here were run using the Parallel Ice Sheet Model (PISM, development version 8ff7cbe), an open source, finite difference, shallow ice sheet model (the PISM authors, 2015). The model requires input on basal topography, sea level, geothermal heat flux and climate forcing. It computes the evolution of ice extent and thickness over time, the thermal and dynamic states of the ice sheet, and the associated lithospheric response.

Basal topography is derived from the ETOPO1 combined topography and bathymetry dataset with a resolution of 1 arc-min (Amante and Eakins, 2009). Sea level is lowered as a function of time based on the Spectral Mapping Project (SPECMAP, Imbrie et al., 1989) time scale. Geothermal heat flux is applied as a constant value of 70 mW m^{-2} at 3 km depth (Sect. 2.2). Surface mass balance is computed using a positive degree-day (PDD) model (Sect. 2.3). Climate forcing is provided by a monthly climatology averaged from 1979 to 2000 from the North American Regional Reanalysis (NARR, Mesinger et al., 2006), perturbated by time-dependent offsets and lapse-rate temperature corrections (Sect. 2.4).

Each simulation starts from assumed ice-free conditions at 120 000 years ago (120 ka), and runs to the present. Our modelling domain of 1500 by 3000 km encompasses the entire area covered by the Cordilleran ice sheet at the LGM (Fig. 1). The simulations were run on two distinct grids, using a lower horizontal resolution of 10 km, and a higher horizontal resolution of 5 km. These computations were performed on 16 to 128 computing cores at the Swedish National Supercomputing Centre.

2.2 Ice thermodynamics

Ice sheet dynamics are typically modelled using a combination of internal deformation and basal sliding. PISM is a shallow ice sheet model, which implies that the balance

TCD
9, 4147–4203, 2015

of stresses is approximated based on their predominant components. The Shallow Shelf Approximation (SSA) is used as a "sliding law" for the Shallow Ice Approximation (SIA) by adding velocity solutions of the two approximations (Bueler and Brown, 2009; Winkelmann et al., 2011, Eqs. 7–9 and 15).

Ice rheology depends on temperature and water content through an enthalpy formulation (Aschwanden et al., 2012). Surface air temperature derived from the climate forcing (Sect. 2.4) provides the upper boundary condition to the ice enthalpy model. Temperature is computed subglacially to a depth of 3 km, where it is conditioned by a lower boundary geothermal heat flux of 70 mW m^{-2}. Although this uniform value does not account for the high spatial geothermal variability in the region (Blackwell and Richards, 2004), it is, on average, representative of available heat flow measurements. In the low-resolution simulations, the vertical grid consists of 31 temperature layers in the bedrock and up to 51 enthalpy layers in the ice sheet, corresponding to a vertical resolution of 100 m. The high-resolution simulations 61 bedrock layers and up to 101 ice layers with a vertical resolution of 50 m.

A pseudo-plastic sliding law,

$$\boldsymbol{\tau}_\mathrm{b} = -\tau_\mathrm{c} \frac{\boldsymbol{v}_\mathrm{b}}{v_\mathrm{th}{}^{q} \, |\boldsymbol{v}_\mathrm{b}|^{1-q}}, \tag{1}$$

relates the bed-parallel shear stresses, $\boldsymbol{\tau}_\mathrm{b}$, to the sliding velocity, $\boldsymbol{v}_\mathrm{b}$ (Table 1). The yield stress, τ_c, is modelled using the Mohr–Coulomb criterion,

$$\tau_\mathrm{c} = c_0 + N \tan\phi, \tag{2}$$

where cohesion, c_0, is assumed to be zero. The friction angle, ϕ, varies from 15 to 45° as a piecewise-linear function of modern bed elevation, with the lowest value occuring below modern sea level (0 m a.s.l.) and the highest value occuring above the generalised elevation of the highest shorelines (200 m a.s.l., Clague, 1981, Fig. 5), thus accounting for a weakening of till associated with the presence of marine sediments (cf. Martin et al., 2011; Aschwanden et al., 2013, Supplement; the PISM authors, 2015).

TCD
9, 4147–4203, 2015

Effective pressure, N, is related to the ice overburden stress, $\rho g h$, and the modelled amount of subglacial water, using a formula derived from laboratory experiments with till extracted from the base of Ice Stream B in West Antarctica (Tulaczyk et al., 2000; Bueler and van Pelt, 2015),

$$N = \delta \rho g h \, 10^{(e_0/C_c)(1-(W/W_{max}))}, \quad (3)$$

where δ is chosen as 0.02, e_0 is a measured reference void ratio and C_c is a measured compressibility coefficient (Table 1). The amount of water at the base, W, varies from zero to $W_{max} = 2$ m, a threshold above which additional melt water is assumed to drain off instantaneously. Finally, the bedrock topography responds to ice load following a bedrock deformation model that includes local isostasy, elastic lithosphere flexure and viscous astenosphere deformation in an infinite half-space (Lingle and Clark, 1985; Bueler et al., 2007). A relatively low viscosity value of $\nu_m = 1 \times 10^{19}$ Pa s is used for the astenosphere (Table 1) in accordance with the results from regional glacial isostatic adjustment modelling at the northern Cascadia subduction zone (James et al., 2009).

Ice shelf calving is computed using a double criterion. First, a physically-realistic calving flux is computed based on eigenvalues of the horizontal strain rate tensor (Winkelmann et al., 2011; Levermann et al., 2012). This allows floating ice to advance in confined embayments, but prevents the formation of extensive ice shelves in the open ocean. Second, floating ice thinner than 50 m is systematically calved off. A subgrid scheme by Albrecht et al. (2011) allows for a continuous migration of the calving front. This formulation of calving has been applied to the Antarctic ice sheet and has shown to produce a realistic calving front positon for many of the present-day ice shelves (Martin et al., 2011).

2.3 Surface mass balance

Ice surface accumulation and ablation are computed from monthly mean near-surface air temperature, T_m, monthly standard deviation of near-surface air temperature, σ, and

TCD
9, 4147–4203, 2015

monthly precipitation, P_m, using a temperature-index model (e.g., Hock, 2003). Accumulation is equal to precipitation when air temperatures are below 0 °C, and decreases to zero linearly with temperatures between 0 and 2 °C. Ablation is computed from PDD, defined as an integral of temperatures above 0 °C in one year.

The PDD computation accounts for stochastic temperature variations by assuming a normal temperature distribution of standard deviation σ aroung the expected value T_m. It is expressed by an error-function formulation (Calov and Greve, 2005),

$$\mathrm{PDD} = \int_{t_1}^{t_2} \mathrm{d}t \left[\frac{\sigma}{\sqrt{2\pi}} \exp\left(-\frac{T_m^2}{2\sigma^2} \right) + \frac{T_m}{2} \operatorname{erfc}\left(-\frac{T_m}{\sqrt{2}\sigma} \right) \right], \tag{4}$$

which is numerically approximated using week-long sub-intervals. In order to account for the effects of spatial and seasonal variations of temperature variability (Seguinot, 2013), σ is computed from NARR daily temperature values from 1979 to 2000 (Mesinger et al., 2006), including variability associated with the seasonal cycle (Fig. 2). Degree-day factors for snow and ice melt are derived from mass-balance measurements on contemporary glaciers from the Coast Mountains and Rocky Mountains in British Columbia (Table 1; Shea et al., 2009).

2.4 Climate forcing

Climate forcing driving ice sheet simulations consists of a present-day monthly climatology, $\{T_{m0}, P_{m0}\}$, where temperatures are modified by offset time series, ΔT_{TS}, and lapse-rate corrections, ΔT_{LR}:

$$T_m(t,x,y) = T_{m0}(x,y) + \Delta T_{TS}(t) + \Delta T_{LR}(t,x,y), \tag{5}$$

$$P_m(t,x,y) = P_{m0}(x,y). \tag{6}$$

The present-day monthly climatology was computed from near-surface air temperature and precipitation rate fields from the NARR, averaged from 1979 to 2000. Modern

TCD
9, 4147–4203, 2015

climate of the North American Cordillera is characterised by strong geographic variations in temperature seasonality, timing of the maximum annual precipitation, and daily temperature variability (Fig. 2). The use of NARR is motivated by the need for an accurate, high-resolution precipitation forcing, as identified in a previous sensitivity study (Seguinot et al., 2014).

Temperature offset time-series, ΔT_{TS}, are derived from palaeo-temperature proxy records from the Greenland Ice Core Project (GRIP, Dansgaard et al., 1993), the North Greenland Ice Core Project (NGRIP, Andersen et al., 2004), the European Project for Ice Coring in Antarctica ‘ =10 2.4 Jouzel.etal.2007, the Vostok ice core (Petit et al., 1999), and Ocean Drilling Program (ODP) sites 1012 and 1020, both located off the coast of California (Herbert et al., 2001). Palaeo-temperature anomalies from the GRIP and NGRIP records were calculated from oxygen isotope ($\delta^{18}\mathrm{O}$) measurements using a quadratic equation (Johnsen et al., 1995),

$$\Delta T_{\mathrm{TS}}(t) = -11.88[\delta^{18}\mathrm{O}(t) - \delta^{18}\mathrm{O}(0)] - 0.1925[\delta^{18}\mathrm{O}(t)^2 - \delta^{18}\mathrm{O}(0)^2], \quad (7)$$

while temperature reconstructions from Antarctic and oceanic cores were provided as such. All records were scaled linearly (Table 2) in order to simulate comparable ice extents at the LGM (Table 3) and realistic outlines (Fig. 4).

Finally, lapse-rate corrections, ΔT_{LR}, are computed as a function of ice surface elevation, s, using the NARR surface geopotential height invariant field as a reference topography, b_{ref}:

$$\Delta T_{\mathrm{LR}}(t,x,y) = -\gamma[s(t,x,y) - b_{\mathrm{ref}}] \quad (8)$$

$$= -\gamma[h(t,x,y) + b(t,x,y) - b_{\mathrm{ref}}], \quad (9)$$

thus accounting for the evolution of ice thickness, $h = s - b$, on the one hand, and for differences between the basal topography of the ice flow model, b, and the NARR reference topography, b_{ref}, on the other hand. All simulations use an annual temperature

TCD
9, 4147–4203, 2015

lapse rate of $\gamma = 6\,\mathrm{K\,km^{-1}}$. In the rest of this paper, we refer to different model runs by the name of the proxy record used for the palaeo-temperature forcing.

3 Sensitivity to climate forcing time-series

3.1 Evolution of ice volume

Despite large differences in the input climate forcing (Fig. 3, upper panel), model output presents consistent features that can be observed across the range of forcing data used. In all simulations, modelled ice volumes remain relatively low during most of the glacial cycle, except during two major glacial events which occur between 61.9 and 56.5 ka during MIS 4, and between 23.2 and 16.8 ka during MIS 2 (Fig. 3, lower panel). An ice volume minimum is consistently reached between 53.0 and 41.3 ka during MIS 3. However, the magnitude and precise timing of these three events depend significantly on the choice of proxy record used to derive a time-dependent climate forcing (Table 3).

Simulations forced by the Greenland ice core palaeo-temperature records (GRIP, NGRIP) produce the highest variability in modelled ice volume throughout the last glacial cycle. In contrast, simulations driven by oceanic (ODP 1012, ODP 1020) and Antarctic (EPICA, Vostok) palaeo-temperature records generally result in lower ice volume variability throughout the simulation length, resulting in lower modelled ice volumes during MIS 4 and larger ice volumes during MIS 3. The NGRIP climate forcing is the only one that results in a larger ice volume during MIS 4 than during MIS 2.

While simulations driven by the GRIP and the two Antarctic palaeo-temperature records attain a last ice volume maximum between 19.1 and 16.8 ka, those informed by the NGRIP and the two oceanic palaeo-temperature records attain their maximum ice volumes thousands of years earlier. Moreover, the ODP 1012 run yields a rapid deglaciation of the modelled area prior to 17 ka. The ODP 1020 simulation predicts an early maximum in ice volume at 23.2 ka, followed by slower deglaciation than modelled

TCD
9, 4147–4203, 2015

using the other palaeo-temperature records. Finally, whereas model runs forced by the Antarctic palaeo-temperature records result in a rapid and uninterrupted deglaciation after the LGM, the simulation driven by the GRIP palaeo-temperature record also results in a rapid deglaciation but in three steps, separated by two periods of ice sheet regrowth (Fig. 3).

3.2 Extreme configurations

Despite large differences in the timing of attained volume extrema (Table 3), all model runs show relatively consistent patterns of glaciation. During MIS 4, all simulations produce an extensive ice sheet, covering an area of at least half of that attained during MIS 2 (Table 3; Fig. 4, upper panels). Corresponding maximum ice volumes also differ significantly between model runs, and vary between 3.84 and 8.84 m sea level equivalents (m s.l.e.; Table 3).

In the MIS 3 ice volume minimum reconstructions, a central ice cap persists over the Skeena Mountains (Fig. 4, middle panels). Although this ice cap is present in all simulations, its dimensions depend sensitively on the choice of the applied palaeo-temperature record. Modelled ice volume minima spread over a wide range between 1.69 and 2.88 m s.l.e. (Table 3).

Modelled ice sheet geometries during the LGM (MIS 2; Fig. 4, lower panels) invariably include a ca. 1500 km-long central divide above 3000 m a.s.l. located along the spine of the Rocky Mountains. Although the similarity of modelled ice extents is a direct result of the choice of scaling factors applied to different palaeo-temperature proxy records (Table 2), it is interesting to note that modelled maximum ice volumes also fall within a tight range of 8.40 to 8.91 m s.l.e. (Table 3).

TCD
9, 4147–4203, 2015

4 Comparison with the geologic record

Large variations in the model responses to evolving climate forcing reveal its sensitivity to the choice of palaeo-temperature proxy record. To distinguish between different records, geological evidence of former glaciations provide a basis for validation of our runs, while the results from numerical modelling can perhaps help to analyse some of the complexity of this evidence. In this section, we compare model outputs to the geologic record, in terms of timing and configuration of the maximum stages, location and lifetime of major nucleation centres, and patterns of ice retreat during the last deglaciation.

4.1 Glacial maxima

4.1.1 Timing of glaciation

Independently of the palaeo-temperature records used to force the ice sheet model, our simulations consistently produce two glacial maxima during the last glacial cycle. The first maximum configuration is obtained during MIS 4 (61.9–56.5 ka) and the second during MIS 2 (23.2–16.8 ka; Figs. 3, 4; Table 3). These events broadly correspond in timing to the Gladstone (MIS 4) and McConnell (MIS 2) glaciations documented by geological evidence for the northern sector of the Cordilleran ice sheet (Duk-Rodkin et al., 1996; Ward et al., 2007; Stroeven et al., 2010, 2014), and to the Fraser Glaciation (MIS 2) documented for its southern sector (Porter and Swanson, 1998; Margold et al., 2014). There is stratigraphical evidence for an MIS 4 glaciation in British Columbia (Clague and Ward, 2011) and in the Puget Lowland (Troost, 2014), but their extent and timing are still highly conjectural (perhaps MIS 4 or early MIS 3; e.g., Cosma et al., 2008).

The exact timing of modelled MIS 2 maximum ice volume depends strongly on the choice of applied palaeo-temperature record, which allows for a more in-depth comparison with geological evidence for the timing of maximum Cordilleran ice sheet

TCD
9, 4147–4203, 2015

extent. In the Puget Lowland (Fig. 1), the LGM advance of the southern Cordilleran ice sheet margin has been constrained by radiocarbon dating on wood between 17.4 and 16.4 ^{14}C cal ka (Porter and Swanson, 1998). These dates are consistent with radiocarbon dates from the offshore sedimentary record, which reveals an increase of glaciomarine sedimentation between 19.5 and 16.2 ^{14}C cal ka (Cosma et al., 2008; Taylor et al., 2014). Radiocarbon dating of the northern Cordilleran ice sheet margin is much less constrained but straddles presented constraints from the southern margin. However, cosmogenic exposure dating places the timing of maximum CIS extent during the McConnell glaciation close to 17 ^{10}Be ka (Stroeven et al., 2010, 2014). A sharp transition in the sediment record of the Gulf of Alaska indicates a retreat of regional outlet glaciers onto land at 14.8 ^{14}C cal ka (Davies et al., 2011).

Among the simulations presented here, only those forced with the GRIP, EPICA and Vostok palaeo-temperature records yield Cordilleran ice sheet maximum extents that may be compatible with these field constraints (Fig. 3, lower panel; Table 3). Simulations driven by the NGRIP, ODP 1012 and ODP 1020 palaeo-temperature records, on the contrary, yield MIS 2 maximum Cordilleran ice sheet volumes that pre-date field-based constraints by several thousands of years (about 6, 6 and 4 ka respectively). Concerning the simulations driven by oceanic records, this early deglaciation is caused by an early warming present in the alkenone palaeo-temperature reconstructions (Fig. 3, upper panel; Herbert et al., 2001, Fig. 3). However, this early warming is a local effect, corresponding to a weakening of the California current (Herbert et al., 2001). The California current, driving cold waters southwards along the southwestern coast of North America, has been shown to have weakened during each peak of global glaciation (in SPECMAP) during the past 550 ka, including the LGM, resulting in paradoxically warmer sea-surface temperatures at the locations of the ODP 1012 and ODP 1020 sites (Herbert et al., 2001).

Because most of the marine margin of the Cordilleran ice sheet terminated in a sector of the Pacific Ocean unaffected by variations in the California current, it probably remained insensitive to this local phenomenum. However, the above paradox illustrates

TCD
9, 4147–4203, 2015

the complexity of ice-sheet feedbacks on regional climate, and demonstrates that, although located in the neighbourhood of the modelling domain, the ODP 1012 and ODP 1020 palaeo-temperature records cannot be used as a realistic forcing to model the Cordilleran ice sheet through the last glacial cycle. Similarly, the simulation using the NGRIP palaeo-temperature record depicts an early onset of deglaciation (Fig. 3) following its last glacial volume maximum (22.9 ka, Table 3) attained about 6 ka earlier than dated evidence of the LGM advance. There is a fair agreement between the EPICA and Vostok palaeo-temperature records, resulting in only small differences between the simulations driven by those records. These differences are not subject to further analysis further; instead we focus on simulations forced by palaeo-temperature records from the GRIP and EPICA ice cores that appear to produce the most realistic reconstructions of regional glaciation history, yet bearing significant disparities in model output. To allow for a more detailed comparison against the geological record, these two simulations were re-run using a higher-resolution grid (Sect. 2; Fig. 3, lower panel, dotted lines).

4.1.2 Ice configuration during MIS 2

During maximum glaciation, both simulations position the main meridional ice divide over the western flank of the Rocky Mountains (Figs. 4, lower panels and 5). This result appears to contrast with palaeoglaciological reconstructions for central and southern British Columbia with ice divides in a more westerly position, over the western margin of the Interior Plateau (Ryder et al., 1991; Stumpf et al., 2000; Kleman et al., 2010; Clague and Ward, 2011; Margold et al., 2013b). These indicate that a latitudinal saddle connected ice dispersal centres in the Columbia Mountains with the main ice divide (Ryder et al., 1991; Kleman et al., 2010; Clague and Ward, 2011; Margold et al., 2013b). A latitudinal saddle does indeed feature in our modelling results, however, in an inverse configuration between the main ice divide over the Columbia Mountains and a secondary divide over the southern Coast Mountains (Fig. 5).

TCD
9, 4147–4203, 2015

Such deviation from the geological inferences could reflect the fact that our model does not include feedback mechanisms between ice sheet topography and the regional climate. Firstly, during the build-up phase preceding the LGM, rapid accumulation over the Coast Mountains enhanced the topographic barrier formed by these mountain ranges, which likely resulted in a decrease of precipitation and, therefore, a decrease of accumulation in the interior. Secondly, latent warming of the moisture-depleted air parcels flowing over this enhanced topography could have resulted in an inflow of potentially warmer air over the eastern flank of the ice sheet, increasing melt along the advancing margin (cf. Langen et al., 2012). Because these two processes, both with a tendency to limit ice-sheet growth, are absent from our model, the eastern margin of the ice sheet and the position of the main meridional ice divide are certainly biased towards the east in our simulations (Seguinot et al., 2014).

However, field-based palaeoglaciological reconstructions have struggled to reconcile the more westerly-centred ice divide in south-central British Columbia with evidence in the Rocky Mountains and beyond, that the Cordilleran ice sheet invaded the western Interior Plains, where it merged with the southwestern margin of the Laurentide ice sheet and was deflected to the south (Jackson et al., 1997; Bednarski and Smith, 2007; Kleman et al., 2010; Margold et al., 2013a, b). Ice geometries from our model runs do not have this problem, because the position and elevation of the ice divide ensure significant ice drainage across the Rocky Mountains at the LGM (Fig. 5).

During MIS 2, the modelled total ice volume peaks at 8.01 m s.l.e. (19.1 ka) in the GRIP simulation and at 8.77 m s.l.e. (17.2 ka) in the EPICA simulation.

4.1.3 Ice configuration during MIS 4

The modelled ice sheet configurations corresponding to ice volume maxima during MIS 4 are more sensitive to the choice of atmospheric forcing than those corresponding to ice volume maxima during MIS 2 (Figs. 4, upper panels and 6). The GRIP simulation (Fig. 6, left panel) results in a modelled maximum ice sheet extent that closely resembles that obtained during MIS 2, with the only major difference of being slightly

TCD
9, 4147–4203, 2015

less extensive across northern and eastern sectors. In contrast, the EPICA simulation produces a lower ice volume maximum (Fig. 3), which translates in the modelled ice sheet geometry into a significantly reduced southern sector, more restricted ice cover in northern and eastern sectors, and generally lower ice surface elevations in the interior (Fig. 6, right panel). Thus, only the GRIP simulation can explain the presence of MIS 4 glacial deposits in the Puget Lowland (Troost, 2014) and that of ice-rafted debris in the marine sediment record offshore Vancouver Island at ca. 47 ^{14}C cal ka (Cosma et al., 2008).

During MIS 4, the modelled total ice volume peaks at 7.19 m s.l.e. (57.3 ka) in the GRIP simulation and at 5.04 m s.l.e. (61.9 ka) in the EPICA simulation, corresponding to respectively 90 and 57 % of modelled MIS 2 ice volumes.

4.2 Nucleation centres

4.2.1 Transient ice sheet states

Palaeo-glaciological reconstructions are generally more robust for maximum ice sheet extents and late ice sheet configurations than for intermediate or minimum ice sheet extents and older ice sheet configurations (Kleman et al., 2010). However, these maximum stages are, by nature, extreme configurations, which do not necessarily represent the dominant patterns of glaciation throughout the period of ice cover (Porter, 1989; Kleman and Stroeven, 1997; Kleman et al., 2008, 2010).

For the Cordilleran ice sheet, geological evidence from radiocarbon dating (Clague et al., 1980; Clague, 1985, 1986; Porter and Swanson, 1998; Menounos et al., 2008), cosmogenic exposure dating (Stroeven et al., 2010, 2014; Margold et al., 2014), bedrock deformation in response to former ice loads (Clague and James, 2002; Clague et al., 2005), and offshore sedimentary records (Cosma et al., 2008; Davies et al., 2011) indicate that the LGM maximum extent was short-lived. To compare this finding to our simulations, we use numerical modelling output to compute durations of ice cover throughout the last glacial cycle (Fig. 7).

TCD
9, 4147–4203, 2015

The resulting maps show that, during most of the glacial cycle, modelled ice cover is restricted to disjoint ice caps centred on major mountain ranges of the North American Cordillera (Fig. 7, blue areas). A 2500 km-long continuous expanse of ice, extending from the Alaska Range in the northeast to the Rocky Mountains in the southwest, is only in operation for at most 32 ka, which is about a third of the timespan of the last glacial cycle (Fig. 7, hatched areas). However, except for its margins in the Pacific Ocean and in the northern foothills of the Alaska Range, the maximum extent of the ice sheet is attained for a much shorter period of time of only few thousand years (Fig. 7, red areas). This result illustrates that the maximum extents of the modelled ice sheet during MIS 4 and MIS 2 were both short-lived and therefore out of balance with contemporary climate.

A notable exception to the transient character of the maximum extent of Cordilleran ice sheet is the northern slope of the Alaska Range, where modelled glaciers are confined to its foothills during the entire simulation period (Fig. 7, AR). This apparent insensitivity of modelled glacial extent to temperature fluctuations results from a combination of low precipitation, high summer temperature and large temperature standard deviation (PDD SD) in the plains of the Alaska Interior (Fig. 2) which confines glaciation to the foothills of the mountains. This result could potentially explain the local distribution of glacial deposits, which indicates that glaciers flowing on the northern slope of the Alaska Range have remained small throughout the Pleistocene (Kaufman and Manley, 2004).

4.2.2 Major ice-dispersal centres

It is generally believed that the Cordilleran ice sheet formed by the coalescence of several mountain-centred ice caps (Davis and Mathews, 1944). In our simulations, major ice-dispersal centres, visible on the modelled ice cover duration maps (Fig. 7), are located over the Coast Mountains (CM), the Columbia and Rocky mountains (CRM), the Skeena Mountains (SM), and the Selwyn and Mackenzie mountains (SMKM). The Wrangell and Saint Elias mountains, heavily glacierized at present, host an ice cap for

TCD
9, 4147–4203, 2015

the entire length of both simulations, but that ice cap does not appear to be a major feed to the Cordilleran ice sheet (Fig. 7, WSEM). Although the Coast, Skeena and Columbia and Rocky mountains (CM, SM, CRM) are covered by mountain glaciers for most of the last glacial cycle, providing durable nucleation centres for an ice sheet, this is not the case for the Selwyn and Mackenzie mountains (SMKM), where ice cover on the highest peaks is limited to a small fraction of the last glacial cycle. In other words, the Selwyn and Mackenzie mountains only appear as a secondary ice-dispersal centre during the coldest periods of the last glacial cycle. The Northern Rocky Mountains (Fig. 7, NRM) do not act as a nucleation centre, but rather as a pinning point for the Cordilleran ice sheet margin coming from the west.

Perhaps the most striking feature displayed by the distributions of modelled ice cover is the persistence of the Skeena Mountains ice cap throughout the entire last glacial period (ca. 100–10 ka) and its predominance over the other ice-dispersal centres (Figs. 4 and 7, SM). Regardless of the applied forcing, this ice cap appears to survive MIS 3 (Fig. 4, middle panels), and serves as a nucleation centre at the onset of the glacial readvance towards the LGM (MIS 2). This situation appear similar to the neighbouring Laurentide ice sheet, for which the importance of residual ice for the glacial history leading up to the LGM has been illustrated by the MIS 3 residual ice bodies in northern and eastern Canada as nucleation centres for a much more extensive MIS 2 configuration (Kleman et al., 2010).

The presence of a Skeena Mountains ice cap during most of the last glacial cycle can be explained by meteorological conditions more favourable for ice growth there than elsewhere. In fact, reanalysed atmospheric fields used to force the surface mass balance model show that high winter precipitations are mainly confined to the western slope of the Coast Mountains, except in the centre of the modelling domain where they also occur further inland than along other east-west transects (Fig. 2). In fact, along most of the north-western coast of North America, coastal mountain ranges form a pronounced topographic barrier for westerly winds, capturing atmospheric moisture in the form of orographic precipitation, and resulting in arid interior lowlands. However, near

TCD
9, 4147–4203, 2015

the centre of our modelling domain, this barrier is less pronounced than elsewhere, allowing westerly winds to carry moisture further inland, until it is captured by the extensive Skeena Mountains in north-central British Columbia, thus resulting in a more widespread distribution of winter precipitation (Fig. 2).

The modelled total ice volume corresponding to these persistent ice-dispersal centres attains a minimum of 1.52 m s.l.e. (42.9 ka) in the GRIP simulation and of 2.68 m s.l.e. (51.8 ka) in the EPICA simulation, corresponding to respectively 19 and 31 % of the MIS 2 ice volumes.

4.2.3 Erosional imprint on the landscape

A correlation is observed between the modelled duration of warm based ice cover (Fig. 8) and the degree of glacial modification of the landscape (mainly in terms of the development of deep glacial valleys and troughs). We find evidence for this on the slopes of the Coast Mountains, the the Columbia and Rocky mountains, the Wrangell and Saint Elias mountains, and radiating off the Skeena Mountains (Figs. 7 and 8; Kleman et al., 2010, Fig. 2). The Skeena Mountains, for example, indeed bear a strong glacial imprint that indicates ice drainage in a system of distinct glacial troughs emanating in a radial pattern from the centre of the mountain range (Kleman et al., 2010, Fig. 2). We suggest that persistent ice cover (Fig. 7) associated with basal ice temperatures at the pressure melting point (Figs. 8 and 9) explains the large-scale glacial erosional imprint on the landscape. A well-developed network of glacial valleys running to the north-west on the west slope of the Selwyn and Mackenzie Mountains (Kleman et al., 2010, Fig. 2; Stroeven et al., 2010, Fig. 8) is modelled to have hosted predominantly warm-based ice (Fig. 9). However, because it is only glaciated for a short fraction of the last glacial cycle in our simulations (Fig. 7), this perhaps indicates that the observed landscape pattern originates from multiple glacial cycles and witnesses an increased relative importance of the Selwyn and Mackenzie mountains ice dispersal centre (Fig. 7, SMKM), prior to the Late Pleistocene (cf. Ward et al., 2008; Demuro et al., 2012).

TCD
9, 4147–4203, 2015

The modelled distribution of warm-based ice cover (Figs. 8 and 9) is inevitably affected by our assumption of a constant, 70 mW m^{-2} geothermal heat flux at 3 km depth (Sect. 2.2). However, the Skeena Mountains and the area west of the Mackenzie Mountains experience higher-than-average geothermal heat flux with measured values of ca. 80 and ca. 100 mW m^{-2} (Blackwell and Richards, 2004). We can therefore expect even longer durations of warm-based ice cover for these areas if we were to include spatially variable geothermal forcing in our Cordilleran ice sheet simulations.

4.3 The last deglaciation

4.3.1 Pace and patterns of deglaciation

Similarly to other glaciated regions, most glacial traces in the North American Cordillera relate to the last few millennia of glaciation, because most of the older evidence has been overprinted by warm-based ice retreat during the last deglaciation (Kleman, 1994; Kleman et al., 2010). From a numerical modelling perspective, phases of glacier retreat are more challenging than phases of growth, because they involve more rapid fluctuations of the ice margin, increased flow velocities and longitudinal stress gradients, and poorly understood hydrological processes. The latter are typically included in the models through simple parametrisations (e.g. Clason et al., 2012, 2014; Bueler and van Pelt, 2015), if included at all. However, next after the mapping of maximum ice sheet extents during MIS 2 and MIS 4 (Sects. 4.1.2 and 4.1.3), geomorphologically-based reconstructions of patterns of ice sheet retreat during the last deglaciation provide the second best source of evidence for the validation of our simulations.

In the North American Cordillera, the presence of lateral meltwater channels at high elevation (Margold et al., 2011, 2013b, 2014), and abundant esker systems at low elevation (Burke et al., 2012a, b; Perkins et al., 2013; Margold et al., 2013a) indicate that meltwater was produced over large portions of the ice sheet surface during deglaciation. The southern and northern margins of the Cordilleran ice sheet reached their last glacial maximum extent around 17 ka (Sect. 4.1.1; Porter and Swanson, 1998; Cosma

TCD
9, 4147–4203, 2015

et al., 2008; Stroeven et al., 2010, 2014), which we take as a limiting age for the onset of ice retreat. The timing of final deglaciation is less well constrained, but recent cosmogenic dates from north-central British Columbia indicate that a seizable ice cap emanating from the central Coast Mountains or the Skeena Mountains persisted into the Younger Dryas chronozone, at least until 12.4 ka (Margold et al., 2014).

In our simulations, the timing of peak ice volume during the LGM and the pacing of deglaciation depend critically on the choice of climate forcing (Table 3; Figs. 3 and 10). Adopting the EPICA climate forcing yields peak ice volume at 17.2 ka and an uninterrupted deglaciation until about 9 ka (Fig. 10, lower panel, red curves). On the contrary, the simulation driven by the GRIP palaeo-temperature record yields peak ice volume at 19.3 ka and a deglaciation interrupted by two phases of regrowth until about 8 ka. The first interruption occurs between 16.6 and 14.5 ka, and the second between 13.1 and 11.6 ka (Fig. 10, lower panel, blue curve).

Hence, the two model runs, while similar in overall timing compared to the runs with other climate drivers, differ in detail. On the one hand, the EPICA run depicts peak glaciation about 2 ka later than the GRIP run, in closer agreement with dated maximum extents, and shows a faster, uninterrupted deglaciation which yields sporadic ice cover more than 1 ka earlier. On the other hand, the GRIP run yields a deglaciation in three steps, compatible with marine sediment sequences offshore Vancouver Island, where the distribution of ice-rafted debris indicates an ice margin retreat from the Georgia Strait in two phases that are contemporary with warming oceanic temperatures from 17.2 to 16.5 and from 15.5 to 14.0 ^{14}C cal ka (Taylor et al., 2014).

Modelled patterns of ice sheet retreat are relatively consistent between the two simulations (Figs. 11 and 12). The southern sector of the modelling domain, including the Puget Lowland, the Coast Mountains, the Columbia and and Rocky mountains, and the Interior Plateau of British Columbia, becomes completely deglaciated by 10 ka, whereas a significant ice cover remains over the Skeena, the Selwyn and Mackenzie, and the Wrangell and Saint Elias mountains in the northern sector of the modelling domain. After 10 ka, deglaciation continues to proceed across the Liard Lowland with

TCD
9, 4147–4203, 2015

a radial ice margin retreat towards the surrounding mountain ranges, consistent with the regional melt water record of the last deglaciation (Margold et al., 2013a). Remaining ice continues to decay by retreating towards the Selwyn and MacKenzie, and Skeena mountains. The last remnants of the Cordilleran ice sheet finally disappear from the Skeena Mountains at 6.5 ka (GRIP) and 6.1 ka (EPICA).

4.3.2 Late-glacial readvance

The possibility of late glacial readvances in the North American Cordillera has been debated for some time (Osborn and Gerloff, 1997), and locally these have been reconstructed and dated. Radiocarbon-dated end moraines in the Fraser and Squamish valleys, off the southern tip of the Coast Mountains, indicate consecutive glacier maxima, or standstills while in overall retreat, one of which corresponds to the Younger Dryas chronozone (Clague et al., 1997; Friele and Clague, 2002a, b; Kovanen, 2002; Kovanen and Easterbrook, 2002). Although most of these moraines characterise independent valley glaciers, that may have been disconnected from the waning Cordilleran ice sheet, the Finlay River area in the Omenica Mountains (Fig. 12, OM) presents a different kind of evidence. There, sharp-crested moraines indicate a late-glacial readvance of local alpine glaciers and, more importantly, their interaction with larger, lingering remnants of the main body of the Cordilleran ice sheet in the valleys (Lakeman et al., 2008). Additional evidence for late-glacial alpine glacier readvances includes moraines in the eastern Coast Mountains, and the Columbia and Rocky mountains (Osborn and Gerloff, 1997; Menounos et al., 2008).

Although further work is needed to constrain the timing of the late-glacial readvance, to assess its extents and geographical distribution, and to identify the potential climatic triggers (Menounos et al., 2008), it is interesting to note that the simulation driven by the GRIP record produces a late-glacial readvance in the Coast Mountains and in the Columbia and Rocky Mountains (Fig. 12, left panel). In addition to matching the location of some local readvances, the GRIP-driven simulation shows that a large remnant of the decaying ice sheet may still have existed at the time of this late-glacial readvance. In

TCD
9, 4147–4203, 2015

contrast, the EPICA-driven simulation produces a nearly-continuous deglaciation with only a tightly restricted late-glacial readvance on the western slopes of the Saint Elias and the Coast mountains (Fig. 12, right panel).

4.3.3 Deglacial flow directions

Because a general tenant in glacial geomorphology is that the majority of landforms (lineations and eskers) are part of the deglacial envelope (terminology from Kleman et al., 2006), having been formed close inside the retreating margin of ice sheets (Boulton and Clark, 1990; Kleman et al., 1997, 2010), we present maps of basal flow directions immediately preceding deglaciation or at the time of cessation of sliding inside a cold-based retreating margin (Fig. 13). The modelled deglacial flow patterns are mostly consistent between the GRIP and EPICA simulations. They depict an active ice sheet retreat in the peripheral areas, followed by stagnant ice decay in some of the interior regions. Several parts of the modelling domain do not experience any basal sliding throughout the deglaciation phase (Fig. 13, hatched areas). This notably includes parts of the Interior Plateau in British Columbia, major portions of the Alaskan sector of the ice sheet, and a tortuous ribbon running from the Northern Rocky Mountains over the Skeena and Selwyn Mountains and into the Mackenzie Mountains.

Patterns of glacial lineations formed in the northern and southern sectors of the Cordilleran ice sheet (Prest et al., 1968; Clague, 1989, Fig. 1.12; Kleman et al., 2010, Fig. 2) show similarities with the patterns of deglacial ice flow from numerical modelling (Fig. 13). In the northern half of the modelling domain, modelled deglacial flow directions depict an active downhill flow as the last remnants of the ice sheet retreat towards mountain ranges. Converging deglacial flow patterns in the Liard Lowland, for instance (Fig. 13), closely resemble the pattern indicated by glacial lineations (Margold et al., 2013a, Fig. 2).

On the Interior Plateau of south-central British Columbia, both simulations produce a retreat of the ice margin towards the north-east (Fig. 12), a pattern which is validated by the geomorphological and stratigraphical record for ancient pro-glacial lakes

TCD
9, 4147–4203, 2015

dammed by the retreating ice sheet (Perkins and Brennand, 2014). However, the two simulations differ in the mode of retreat. The GRIP simulation yields an active retreat with basal sliding towards the ice margin to the south, whereas the EPICA simulation produces negligible basal sliding on the plateau during deglaciation (Fig. 13). Yet, the Interior Plateau also hosts an impressive set of glacial lineations which indicate a substantial eastwards flow component of the Cordilleran ice sheet (Prest et al., 1968; Kleman et al., 2010). This Interior Plateau lineation set could therefore present a smoking gun for the reliability of the presented model results. One explanation for the incongruent results could be that the missing feedback mechanisms between ice sheet topography and regional climate resulted in a modelled ice divide of the LGM ice sheet beingtoo far to the east (Sect. 4.1.2; Fig. 5; Seguinot et al., 2014). A more westerly-located LGM ice divide would certainly result in a different deglacial flow pattern over the Interior Plateau. However, a more westerly-positioned LGM ice divide would certainly be associated with a thinner ice sheet than that modelled here. Decreased ice thickness would not promote warm-based conditions but, on the contrary, enlarge the region of negligible basal sliding (Fig. 13). Thus, a second explanation for the incongruent results could be that the Interior Plateau lineation system predates deglaciation ice flow, as perhaps indicated by some eskers that appear incompatible with these glacial lineations (Margold et al., 2013b, Fig. 9). Finally, a third explanation could be that local geothermal heat associated with volcanic activity on the Interior Plateau could have triggered the basal sliding (cf. Greenland ice sheet; Fahnestock et al., 2001).

The modelled deglaciation of the Interior Plateau of British Columbia consists of a rapid northwards retreat (Fig. 12) of southwards-flowing non-sliding ice lobes (Fig. 13) positioned in-between deglaciated mountain ranges (Figs. 14 and 15). This result appears compatible with the prevailing conceptual model of deglaciation of central British Columbia, in which mountain ranges emerge from the ice before the plateau (Fulton, 1991, Fig. 7). However, due to different topographic and climatic conditions, our simulations produce different deglaciation patterns in the northern half of the model domain,

TCD
9, 4147–4203, 2015

indicating that this conceptual model may not be applied to the entire area formerly covered by the Cordilleran ice sheet.

5 Conclusions

Numerical simulations of the Cordilleran ice sheet through the last glacial cycle presented in this study consistently produce two glacial maxima during MIS 4 (61.9–56.5 ka, 3.8–8.8 m s.l.e.) and MIS 2 (23.2–16.8 ka, 8.40–8.91 m s.l.e.), two periods corresponding to documented extensive glaciations. This result is independent of the palaeo-temperature record used among the six selected for this study, and thus can be regarded as a robust model output, which broadly matches geological evidence. However, the timing of the two glaciation peaks depends sensitively on which climate record is used to drive the model. The timing of the LGM is best reproduced by the EPICA and Vostok Antarctic ice core records. It occurs about 2 ka too early in the simulation forced by the GRIP ice core record, and occurs even earlier in all other simulations. The mismatch is largest for the two Northwest Pacific ODP palaeo-temperature records, which are affected by the weakening of the California current during the LGM.

In all simulations presented here, ice cover is limited to disjoint mountain ice caps during most of the glacial cycle. The most persistent nucleation centres are located in the Coast Mountains, the Columbia and Rocky mountains, the Selwyn and Mackenzie mountains, and most importantly, in the Skeena Mountains. Throughout the modelled last glacial cycle, the Skeena Mountains host an ice cap which appears to be fed by the moisture intruding inland from the west through a topographic breach in the Coast Mountains. The Skeena ice cap acts as the main nucleation centre for the glacial reavance towards the LGM configuration. As indicated by persistent, warm-based ice in the model, this ice cap perhaps explains the distinct glacial erosional imprint observed on the landscape of the Skeena Mountains.

During deglaciation, none of the climate records used can be selected as producing an optimal agreement between the model results and the geological evidence.

TCD
9, 4147–4203, 2015

Although the EPICA-driven simulation yields the most realistic timing of the LGM and, therefore, start of deglaciation, only the GRIP-driven simulation produces late glacial readvances in areas where these have been documented. Nonetheless, the patterns of ice sheet retreat are consistent between the two simulations, and show a rapid deglaciation of the southern sector of the ice sheet, including a rapid northwards retreat across the Interior Plateau of central British Columbia. The GRIP-driven simulation then produces a late-glacial readvance of local ice caps and of the main body of the decaying Cordilleran ice sheet primarily in the Coast and the Columbia and Rocky Mountains. In both simulations, this is followed by an opening of the Liard Lowland, and a final retreat of the remaining ice caps towards the Selwyn and, finally, the Skeena mountains, which hosts the last remnant of the ice sheet during the middle Holocene (6.6–6.2 ka). Our results identify the Skeena Mountains as a key area to understanding glacial dynamics of the Cordilleran ice sheet, highlighting the need for further geological investigation of this region.

The Supplement related to this article is available online at doi:10.5194/tcd-9-4147-2015-supplement.

Author contributions. J. Seguinot ran the simulations; I. Rogozhina guided experiment design; A. P. Stroeven, M. Margold and J. Kleman took part in the interpretation and comparison of model results against geological evidence. All authors contributed to the text.

Acknowledgements. Foremost, we would like to thank Shawn Marshall for providing a detailed, constructive analysis of this study during J. Seguinot's PhD defence (September 2014). His comments were used to improve the model set-up. We are very thankful to Constantine Khroulev, Ed Bueler, and Andy Aschwanden for providing constant help and development with PISM. This work was supported by the Swedish Research Council (VR) grant no. 2008-3449 to A. P. Stroeven and by the German Academic Exchange Service (DAAD) grant no. 50015537 and a Knut and Alice Wallenberg Foundation grant to J. Seguinot. Computer resources were provided by the Swedish National Infrastructure for Computing (SNIC) allocation no. 2013/1-159 and 2014/1-159 to A. P. Stroeven at the National Supercomputing Center (NSC).

TCD
9, 4147–4203, 2015

References

Albrecht, T., Martin, M., Haseloff, M., Winkelmann, R., and Levermann, A.: Parameterization for subgrid-scale motion of ice-shelf calving fronts, The Cryosphere, 5, 35–44, doi:10.5194/tc-5-35-2011, 2011. 4154

Amante, C. and Eakins, B. W.: ETOPO1 1 arc-minute global relief model: procedures, data sources and analysis, NOAA technical memorandum NESDIS NGDC-24, Natl. Geophys. Data Center, NOAA, Boulder, CO, doi:10.7289/V5C8276M, 2009. 4152, 4189

Andersen, K. K., Azuma, N., Barnola, J.-M., Bigler, M., Biscaye, P., Caillon, N., Chappellaz, J., Clausen, H. B., Dahl-Jensen, D., Fischer, H., Flückiger, J., Fritzsche, D., Fujii, Y., Goto-Azuma, K., Grønvold, K., Gundestrup, N. S., Hansson, M., Huber, C., Hvidberg, C. S., Johnsen, S. J., Jonsell, U., Jouzel, J., Kipfstuhl, S., Landais, A., Leuenberger, M., Lorrain, R., Masson-Delmotte, V., Miller, H., Motoyama, H., Narita, H., Popp, T., Rasmussen, S. O., Raynaud, D., Rothlisberger, R., Ruth, U., Samyn, D., Schwander, J., Shoji, H., Siggard-Andersen, M.-L., Steffensen, J. P., Stocker, T., Sveinbjörnsdóttir, A. E., Svensson, A., Takata, M., Tison, J.-L., Thorsteinsson, T., Watanabe, O., Wilhelms, F., and White, J. W. C.: High-resolution record of Northern Hemisphere climate extending into the last interglacial period, Nature, 431, 147–151, doi:10.1038/nature02805, data archived at the World Data Center for Paleoclimatology, Boulder, Colorado, USA, 2004. 4151, 4156, 4187

Aschwanden, A., Bueler, E., Khroulev, C., and Blatter, H.: An enthalpy formulation for glaciers and ice sheets, J. Glaciol., 58, 441–457, doi:10.3189/2012JoG11J088, 2012. 4153

Aschwanden, A., Aðalgeirsdóttir, G., and Khroulev, C.: Hindcasting to measure ice sheet model sensitivity to initial states, The Cryosphere, 7, 1083–1093, doi:10.5194/tc-7-1083-2013, 2013. 4153

Balay, S., Abhyankar, S., Adams, M. F., Brown, J., Brune, P., Buschelman, K., Eijkhout, V., Gropp, W. D., Kaushik, D., Knepley, M. G., McInnes, L. C., Rupp, K., Smith, B. F., and Zhang, H.: PETSc Web page, available at: http://www.mcs.anl.gov/petsc (last access: 2015), 2015. 4151

Barendregt, R. W. and Irving, E.: Changes in the extent of North American ice sheets during the late Cenozoic, Can. J. Earth Sci., 35, 504–509, doi:10.1139/e97-126, 1998. 4149

Bednarski, J. M. and Smith, I. R.: Laurentide and montane glaciation along the Rocky Mountain Foothills of northeastern British Columbia, Can. J. Earth Sci., 44, 445–457, doi:10.1139/e06-095, 2007. 4162

TCD
9, 4147–4203, 2015

Blackwell, D. D. and Richards, M.: Geothermal Map of North America, Am. Assoc. Petr. Geol., Tulsa, OK, 2004. 4153, 4167

Booth, D. B., Troost, K. G., Clague, J. J., and Waitt, R. B.: The Cordilleran ice sheet, in: The Quaternary Period in the United States, edited by: Gillespie, A., Porter, S., and Atwater, B., vol. 1 of Dev. Quaternary Sci., Elsevier, Amsterdam, 17–43, doi:10.1016/s1571-0866(03)01002-9, 2003. 4149

Boulton, G. S. and Clark, C. D.: A highly mobile Laurentide ice sheet revealed by satellite images of glacial lineations, Nature, 346, 813–817, doi:10.1038/346813a0, 1990. 4170

Boulton, G. S., Dongelmans, P., Punkari, M., and Broadgate, M.: Palaeoglaciology of an ice sheet through a glacial cycle: the European ice sheet through the Weichselian, Quaternary Res., 20, 591–625, doi:10.1016/s0277-3791(00)00160-8, 2001. 4150

Briner, J. P. and Kaufman, D. S.: Late Pleistocene mountain glaciation in Alaska: key chronologies, J. Quaternary Sci., 23, 659–670, doi:10.1002/jqs.1196, 2008. 4149

Bueler, E. and Brown, J.: Shallow shelf approximation as a "sliding law" in a thermodynamically coupled ice sheet model, J. Geophys. Res., 114, F03008, doi:10.1029/2008JF001179, 2009. 4151, 4153

Bueler, E. and van Pelt, W.: Mass-conserving subglacial hydrology in the Parallel Ice Sheet Model version 0.6, Geosci. Model Dev., 8, 1613–1635, doi:10.5194/gmd-8-1613-2015, 2015. 4154, 4167

Bueler, E., Lingle, C. S., and Brown, J.: Fast computation of a viscoelastic deformable Earth model for ice-sheet simulations, Ann. Glaciol., 46, 97–105, doi:10.3189/172756407782871567, 2007. 4154

Burke, M. J., Brennand, T. A., and Perkins, A. J.: Transient subglacial hydrology of a thin ice sheet: insights from the Chasm esker, British Columbia, Canada, Quaternary Res., 58, 30–55, doi:10.1016/j.quascirev.2012.09.004, 2012a. 4167

Burke, M. J., Brennand, T. A., and Perkins, A. J.: Evolution of the subglacial hydrologic system beneath the rapidly decaying Cordilleran Ice Sheet caused by ice-dammed lake drainage: implications for meltwater-induced ice acceleration, Quaternary Res., 50, 125–140, doi:10.1016/j.quascirev.2012.07.005, 2012b. 4167

Calov, R. and Greve, R.: A semi-analytical solution for the positive degree-day model with stochastic temperature variations, J. Glaciol., 51, 173–175, doi:10.3189/172756505781829601, 2005. 4155

TCD
9, 4147–4203, 2015

Carlson, A. E. and Clark, P. U.: Ice sheet sources of sea level rise and freshwater discharge during the last deglaciation, Rev. Geophys., 50, RG4007, doi:10.1029/2011rg000371, 2012. 4149

Carrara, P. E., Kiver, E. P., and Stradling, D. F.: The southern limit of Cordilleran ice in the Colville and Pend Oreille valleys of northeastern Washington during the Late Wisconsin glaciation, Can. J. Earth Sci., 33, 769–778, doi:10.1139/e96-059, 1996. 4149

Clague, J., Armstrong, J., and Mathews, W.: Advance of the late Wisconsin Cordilleran Ice Sheet in southern British Columbia since 22 000 yr BP, Quaternary Res., 13, 322–326, doi:10.1016/0033-5894(80)90060-5, 1980. 4149, 4163

Clague, J. J.: Late Quaternary Geology and Geochronology of British Columbia Part 2: Summary and Discussion of Radiocarbon-Dated Quaternary History, Geol. Surv. of Can., Ottawa, ON, Paper 80-35, doi:10.4095/119439, 1981. 4153

Clague, J. J.: Delaciation of the Prince Rupert – Kitimat area, British Columbia, Can. J. Earth Sci., 22, 256–265, doi:10.1139/e85-022, 1985. 4149, 4163

Clague, J. J.: The Quaternary stratigraphic record of British Columbia — evidence for episodic sedimentation and erosion controlled by glaciation, Can. J. Earth Sci., 23, 885–894, doi:10.1139/e86-090, 1986. 4149, 4163

Clague, J. J.: Character and distribution of Quaternary deposits (Canadian Cordillera), in: Quaternary Geology of Canada and Greenland, edited by: Fulton, R. J., vol. 1 of Geology of Canada, Geol. Surv. of Can., Ottawa, ON, 34–48, doi:10.4095/127905, 1989. 4149, 4170

Clague, J. J. and James, T. S.: History and isostatic effects of the last ice sheet in southern British Columbia, Quaternary Res., 21, 71–87, doi:10.1016/s0277-3791(01)00070-1, 2002. 4149, 4163

Clague, J. J. and Ward, B.: Pleistocene Glaciation of British Columbia, in: Dev. Quaternary Sci., vol. 15, edited by: Ehlers, J., Gibbard, P. L., and Hughes, P. D., Elsevier, Amsterdam, 563–573, doi:10.1016/b978-0-444-53447-7.00044-1, 2011. 4159, 4161

Clague, J. J., Mathewes, R. W., Guilbault, J.-P., Hutchinson, I., and Ricketts, B. D.: Pre-Younger Dryas resurgence of the southwestern margin of the Cordilleran ice sheet, British Columbia, Canada, Boreas, 26, 261–278, doi:10.1111/j.1502-3885.1997.tb00855.x, 1997. 4150, 4169

Clague, J. J., Froese, D., Hutchinson, I., James, T. S., and Simon, K. M.: Early growth of the last Cordilleran ice sheet deduced from glacio-isostatic depression in southwest British Columbia, Canada, Quaternary Res., 63, 53–59, doi:10.1016/j.yqres.2004.09.007, 2005. 4149, 4163

TCD
9, 4147–4203, 2015

Clark, P. U. and Mix, A. C.: Ice sheets and sea level of the Last Glacial Maximum, Quaternary Res., 21, 1–7, doi:10.1016/s0277-3791(01)00118-4, 2002. 4149

Clason, C., Mair, D. W., Burgess, D. O., and Nienow, P. W.: Modelling the delivery of supraglacial meltwater to the ice/bed interface: application to southwest Devon Ice Cap, Nunavut, Canada, J. Glaciol., 58, 361–374, doi:10.3189/2012jog11j129, 2012. 4167

Clason, C., Applegate, P., and Holmlund, P.: Modelling Late Weichselian evolution of the Eurasian ice sheets forced by surface meltwater-enhanced basal sliding, J. Glaciol., 60, 29–40, doi:10.3189/2014jog13j037, 2014. 4167

Cosma, T., Hendy, I., and Chang, A.: Chronological constraints on Cordilleran Ice Sheet glaciomarine sedimentation from core MD02-2496 off Vancouver Island (western Canada), Quaternary Sci. Rev., 27, 941–955, doi:10.1016/j.quascirev.2008.01.013, 2008. 4149, 4159, 4160, 4163, 4167

Dansgaard, W., Johnsen, S. J., Clausen, H. B., Dahl-Jensen, D., Gundestrup, N. S., Hammer, C. U., Hvidberg, C. S., Steffensen, J. P., Sveinbjörnsdottir, A. E., Jouzel, J., and Bond, G.: Evidence for general instability of past climate from a 250-kyr ice-core record, Nature, 364, 218–220, doi:10.1038/364218a0, data archived at the World Data Center for Paleoclimatology, Boulder, Colorado, USA., 1993. 4151, 4156, 4187

Davies, M. H., Mix, A. C., Stoner, J. S., Addison, J. A., Jaeger, J., Finney, B., and Wiest, J.: The deglacial transition on the southeastern Alaska Margin: Meltwater input, sea level rise, marine productivity, and sedimentary anoxia, Paleoceanography, 26, PA2223, doi:10.1029/2010pa002051, 2011. 4149, 4160, 4163

Davis, N. F. G. and Mathews, W. H.: Four phases of glaciation with illustrations from Southwestern British Columbia, J. Geol., 52, 403–413, doi:10.1086/625236, 1944. 4164

Dawson, G. M.: III. – Recent observations on the glaciation of British Columbia and adjacent regions, Geol. Mag., 5, 347–350, doi:10.1017/s0016756800182159, 1888. 4148

Demuro, M., Froese, D. G., Arnold, L. J., and Roberts, R. G.: Single-grain OSL dating of glaciofluvial quartz constrains Reid glaciation in NW Canada to MIS 6, Quaternary Res., 77, 305–316, doi:10.1016/j.yqres.2011.11.009, 2012. 4166

Duk-Rodkin, A.: Glacial limits map of Yukon Territory, Open File 3694, Geol. Surv. of Can., Ottawa, ON, doi:10.4095/210739, 1999. 4149

Duk-Rodkin, A., Barendregt, R. W., Tarnocai, C., and Phillips, F. M.: Late Tertiary to late Quaternary record in the Mackenzie Mountains, Northwest Territories, Canada: stratigraphy, pale-

TCD
9, 4147–4203, 2015

osols, paleomagnetism, and chlorine-36, Can. J. Earth Sci., 33, 875–895, doi:10.1139/e96-066, 1996. 4159
Dyke, A. S.: An outline of North American deglaciation with emphasis on central and northern Canada, in: Dev. Quaternary Sci., vol. 2, edited by: Ehlers, J. and Gibbard, P. L., Elsevier, Amsterdam, 373–424, doi:10.1016/S1571-0866(04)80209-4, 2004. 4149, 4189
Dyke, A. S. and Prest, V. K.: Late wisconsinan and holocene history of the laurentide ice sheet, Geogr. Phys. Quatern., 41, 237–263, doi:10.7202/032681ar, 1987. 4150
Dyke, A. S., Moore, A., and Robertson, L.: Deglaciation of North America, Open File 1547, Geol. Surv. of Can., Ottawa, ON, 2003. 4150
Ehlers, J. and Gibbard, P. L. (Eds.): Dev. Quaternary Sci., vol. 2, Elsevier, Amsterdam, 2004.
Ehlers, J., Gibbard, P. L., and Hughes, P. D. (Eds.): Dev. Quaternary Sci., vol. 15, Elsevier, Amsterdam, 2011.
Fahnestock, M., Abdalati, W., Joughin, I., Brozena, J., and Gogineni, P.: High geothermal heat flow, basal melt, and the origin of rapid ice flow in central greenland, Sience, 294, 2338–2342, doi:10.1126/science.1065370, 2001. 4171
Friele, P. A. and Clague, J. J.: Readvance of glaciers in the British Columbia Coast Mountains at the end of the last glaciation, Quatern. Int., 87, 45–58, doi:10.1016/s1040-6182(01)00061-1, 2002a. 4150, 4169
Friele, P. A. and Clague, J. J.: Younger Dryas readvance in Squamish river valley, southern Coast mountains, British Columbia, Quaternary Res., 21, 1925–1933, doi:10.1016/s0277-3791(02)00081-1, 2002b. 4150, 4169
Fulton, R. J.: Deglaciation studies in Kamloops region, an area of moderate relief, British Columbia, vol. 154 of Bull., Geol. Surv. of Can., Ottawa, ON, doi:10.4095/101467, 1967. 4149
Fulton, R. J.: A Conceptual model for growth and decay of the Cordilleran Ice Sheet, Geogr. Phys. Quatern., 45, 281–286, doi:10.7202/032875ar, 1991. 4149, 4171
Golledge, N. R., Mackintosh, A. N., Anderson, B. M., Buckley, K. M., Doughty, A. M., Barrell, D. J., Denton, G. H., Vandergoes, M. J., Andersen, B. G., and Schaefer, J. M.: Last Glacial Maximum climate in New Zealand inferred from a modelled Southern Alps icefield, Quaternary Res., 46, 30–45, doi:10.1016/j.quascirev.2012.05.004, 2012. 4151
Herbert, T. D., Schuffert, J. D., Andreasen, D., Heusser, L., Lyle, M., Mix, A., Ravelo, A. C., Stott, L. D., and Herguera, J. C.: Collapse of the California current during glacial maxima linked to climate change on land, Sience, 293, 71–76, doi:10.1126/science.1059209, data

TCD
9, 4147–4203, 2015

archived at the World Data Center for Paleoclimatology, Boulder, Colorado, USA, 2001. 4151, 4156, 4160, 4187

Hidy, A. J., Gosse, J. C., Froese, D. G., Bond, J. D., and Rood, D. H.: A latest Pliocene age for the earliest and most extensive Cordilleran Ice Sheet in northwestern Canada, Quaternary Res., 61, 77–84, doi:10.1016/j.quascirev.2012.11.009, 2013. 4149

Hock, R.: Temperature index melt modelling in mountain areas, J. Hydrol., 282, 104–115, doi:10.1016/S0022-1694(03)00257-9, 2003. 4155

Imbrie, J., McIntyre, A., and Mix, A.: Oceanic response to orbital forcing in the late quaternary: observational and experimental strategies, in: Climate and Geo-Sciences, edited by: Berger, A., Schneider, S., and Duplessy, J., vol. 285 of NATO ASI Series C, Kluwer, Norwell, MA, 121–164, doi:10.1007/978-94-009-2446-8_7, 1989. 4152

Ivy-Ochs, S., Schluchter, C., Kubik, P. W., and Denton, G. H.: Moraine exposure dates imply synchronous Younger Dryas Glacier advances in the European Alps and in the Southern Alps of New Zealand, Geogr. Ann. A, 81, 313–323, doi:10.1111/1468-0459.00060, 1999. 4150

Jackson, L. E. and Clague, J. J.: The Cordilleran ice sheet: one hundred and fifty years of exploration and discovery, Geogr. Phys. Quatern., 45, 269–280, doi:10.7202/032874ar, 1991. 4149, 4150

Jackson, L. E., Phillips, F. M., Shimamura, K., and Little, E. C.: Cosmogenic ^{36}Cl dating of the Foothills erratics train, Alberta, Canada, Geology, 25, 195, doi:10.1130/0091-7613(1997)025<0195:ccdotf>2.3.co;2, 1997. 4162

James, T. S., Gowan, E. J., Wada, I., and Wang, K.: Viscosity of the asthenosphere from glacial isostatic adjustment and subduction dynamics at the northern Cascadia subduction zone, British Columbia, Canada, J. Geophys. Res., 114, B04405, doi:10.1029/2008jb006077, 2009. 4154

Johnsen, S. J., Dahl-Jensen, D., Dansgaard, W., and Gundestrup, N.: Greenland palaeotemperatures derived from GRIP bore hole temperature and ice core isotope profiles, Tellus B, 47, 624–629, doi:10.1034/j.1600-0889.47.issue5.9.x, 1995. 4156

Jouzel, J., Masson-Delmotte, V., Cattani, O., Dreyfus, G., Falourd, S., Hoffmann, G., Minster, B., Nouet, J., Barnola, J. M., Chappellaz, J., Fischer, H., Gallet, J. C., Johnsen, S., Leuenberger, M., Loulergue, L., Luethi, D., Oerter, H., Parrenin, F., Raisbeck, G., Raynaud, D., Schilt, A., Schwander, J., Selmo, E., Souchez, R., Spahni, R., Stauffer, B., Steffensen, J. P., Stenni, B., Stocker, T. F., Tison, J. L., Werner, M., and Wolff, E. W.: Orbital and

TCD
9, 4147–4203, 2015

millennial antarctic climate variability over the past 800 000 years, Sience, 317, 793–796, doi:10.1126/science.1141038, data archived at the World Data Center for Paleoclimatology, Boulder, Colorado, USA., 2007. 4151, 4187
Kaufman, D. S. and Manley, W. F.: Pleistocene maximum and late wisconsinan glacier extents across Alaska, USA, in: Dev. Quaternary Sci., vol. 2, edited by: Ehlers, J. and Gibbard, P. L., Elsevier, Amsterdam, 9–27, doi:10.1016/S1571-0866(04)80182-9, 2004. 4164
Kleman, J.: Preservation of landforms under ice sheets and ice caps, Geomorphology, 9, 19–32, doi:10.1016/0169-555x(94)90028-0, 1994. 4167
Kleman, J. and Stroeven, A. P.: Preglacial surface remnants and Quaternary glacial regimes in northwestern Sweden, Geomorphology, 19, 35–54, doi:10.1016/s0169-555x(96)00046-3, 1997. 4163
Kleman, J., Hättestrand, C., Borgström, I., and Stroeven, A.: Fennoscandian paleoglaciology reconstructed using a glacial geological inversion model, J. Glaciol., 43, 283–299, 1997. 4150, 4170
Kleman, J., Hättestrand, C., Stroeven, A. P., Jansson, K. N., De Angelis, H., and Borgström, I.: Reconstruction of palaeo-ice sheets – inversion of their glacial geomorphological record, in: Glacier Science and Environmental Change, edited by: Knight, P. G., Blackwell, Malden, MA, 192–198, doi:10.1002/9780470750636.ch38, 2006. 4170
Kleman, J., Stroeven, A. P., and Lundqvist, J.: Patterns of quaternary ice sheet erosion and deposition in Fennoscandia and a theoretical framework for explanation, Geomorphology, 97, 73–90, doi:10.1016/j.geomorph.2007.02.049, 2008. 4163
Kleman, J., Jansson, K., De Angelis, H., Stroeven, A., Hättestrand, C., Alm, G., and Glasser, N.: North American ice sheet build-up during the last glacial cycle, 115–21 kyr, Quaternary Sci. Rev., 29, 2036–2051, doi:10.1016/j.quascirev.2010.04.021, 2010. 4149, 4150, 4161, 4162, 4163, 4165, 4166, 4167, 4170, 4171
Kovanen, D. J.: Morphologic and stratigraphic evidence for Allerød and Younger Dryas age glacier fluctuations of the Cordilleran Ice Sheet, British Columbia, Canada and Northwest Washington, USA, Boreas, 31, 163–184, doi:10.1111/j.1502-3885.2002.tb01064.x, 2002. 4150, 4169
Kovanen, D. J. and Easterbrook, D. J.: Timing and extent of Allerød and Younger Dryas age (ca. 12 500–10 000 ^{14}C yr BP) oscillations of the Cordilleran Ice Sheet in the Fraser Lowland, Western North America, Quaternary Res., 57, 208–224, doi:10.1006/qres.2001.2307, 2002. 4150, 4169

TCD
9, 4147–4203, 2015

Lakeman, T. R., Clague, J. J., and Menounos, B.: Advance of alpine glaciers during final retreat of the Cordilleran ice sheet in the Finlay River area, northern British Columbia, Canada, Quaternary Res., 69, 188–200, doi:10.1016/j.yqres.2008.01.002, 2008. 4150, 4169

Langen, P. L., Solgaard, A. M., and Hvidberg, C. S.: Self-inhibiting growth of the Greenland ice sheet, Geophys. Res. Lett., 39, L12502, doi:10.1029/2012GL051810, 2012. 4162

Levermann, A., Albrecht, T., Winkelmann, R., Martin, M. A., Haseloff, M., and Joughin, I.: Kinematic first-order calving law implies potential for abrupt ice-shelf retreat, The Cryosphere, 6, 273–286, doi:10.5194/tc-6-273-2012, 2012. 4154

Lingle, C. S. and Clark, J. A.: A numerical model of interactions between a marine ice sheet and the Solid Earth: application to a West Antarctic ice stream, J. Geophys. Res., 90, 1100–1114, doi:10.1029/JC090iC01p01100, 1985. 4154

Lisiecki, L. E. and Raymo, M. E.: A Pliocene-Pleistocene stack of 57 globally distributed benthic δ^{18}O records, Paleoceanography, 20, PA1003, doi:10.1029/2004pa001071, 2005. 4191

Lundqvist, J.: Glaciodynamics of the Younger Dryas Marginal zone in Scandinavia: implications of a revised glaciation model, Geogr. Ann. A, 69, 305, doi:10.2307/521191, 1987. 4150

Margold, M., Jansson, K. N., Kleman, J., and Stroeven, A. P.: Glacial meltwater landforms of central British Columbia, J. Maps, 7, 486–506, doi:10.4113/jom.2011.1205, 2011. 4149, 4167

Margold, M., Jansson, K. N., Kleman, J., and Stroeven, A. P.: Lateglacial ice dynamics of the Cordilleran Ice Sheet in northern British Columbia and southern Yukon Territory: retreat pattern of the Liard Lobe reconstructed from the glacial landform record, J. Quaternary Sci., 28, 180–188, doi:10.1002/jqs.2604, 2013a. 4150, 4162, 4167, 4169, 4170

Margold, M., Jansson, K. N., Kleman, J., Stroeven, A. P., and Clague, J. J.: Retreat pattern of the Cordilleran Ice Sheet in central British Columbia at the end of the last glaciation reconstructed from glacial meltwater landforms, Boreas, 42, 830–847, doi:10.1111/bor.12007, 2013b. 4149, 4161, 4162, 4167, 4171

Margold, M., Stroeven, A. P., Clague, J. J., and Heyman, J.: Timing of terminal Pleistocene deglaciation at high elevations in southern and central British Columbia constrained by ^{10}Be exposure dating, Quaternary Res., 99, 193–202, doi:10.1016/j.quascirev.2014.06.027, 2014. 4149, 4159, 4163, 4167, 4168

Marshall, S. J., Tarasov, L., Clarke, G. K., and Peltier, W. R.: Glaciological reconstruction of the Laurentide Ice Sheet: physical processes and modelling challenges, Can. J. Earth Sci., 37, 769–793, doi:10.1139/e99-113, 2000. 4151

TCD
9, 4147–4203, 2015

Martin, M. A., Winkelmann, R., Haseloff, M., Albrecht, T., Bueler, E., Khroulev, C., and Levermann, A.: The Potsdam Parallel Ice Sheet Model (PISM-PIK) – Part 2: Dynamic equilibrium simulation of the Antarctic ice sheet, The Cryosphere, 5, 727–740, doi:10.5194/tc-5-727-2011, 2011. 4153, 4154

Menounos, B., Osborn, G., Clague, J. J., and Luckman, B. H.: Latest Pleistocene and Holocene glacier fluctuations in western Canada, Quaternary Sci. Rev., 28, 2049–2074, doi:10.1016/j.quascirev.2008.10.018, 2008. 4149, 4150, 4163, 4169

Mesinger, F., DiMego, G., Kalnay, E., Mitchell, K., Shafran, P. C., Ebisuzaki, W., Jović, D., Woollen, J., Rogers, E., Berbery, E. H., Ek, M. B., Fan, Y., Grumbine, R., Higgins, W., Li, H., Lin, Y., Manikin, G., Parrish, D., and Shi, W.: North American regional reanalysis, B. Am. Meteorol. Soc., 87, 343–360, doi:10.1175/BAMS-87-3-343, 2006. 4151, 4152, 4155, 4190

Osborn, G. and Gerloff, L.: Latest pleistocene and early Holocene fluctuations of glaciers in the Canadian and northern American Rockies, Quatern. Int., 38–39, 7–19, doi:10.1016/s1040-6182(96)00026-2, 1997. 4169

Patterson, T. and Kelso, N. V.: Natural Earth, Free vector and raster map data, available at: http://naturalearthdata.com (last access: 2015), 2015. 4189

Perkins, A. J. and Brennand, T. A.: Refining the pattern and style of Cordilleran Ice Sheet retreat: palaeogeography, evolution and implications of lateglacial ice-dammed lake systems on the southern Fraser Plateau, British Columbia, Canada, Boreas, 44, 319–342, doi:10.1111/bor.12100, 2014. 4171

Perkins, A. J., Brennand, T. A., and Burke, M. J.: Genesis of an esker-like ridge over the southern Fraser Plateau, British Columbia: implications for paleo-ice sheet reconstruction based on geomorphic inversion, Geomorphology, 190, 27–39, doi:10.1016/j.geomorph.2013.02.005, 2013. 4167

Petit, J. R., Jouzel, J., Raynaud, D., Barkov, N. I., Barnola, J.-M., Basile, I., Bender, M., Chappellaz, J., Davis, M., Delaygue, G., Delmotte, M., Kotlyakov, V. M., Legrand, M., Lipenkov, V. Y., Lorius, C., Pépin, L., Ritz, C., Saltzman, E., and Stievenard, M.: Climate and atmospheric history of the past 420,000 years from the Vostok ice core, Antarctica, Nature, 399, 429–436, doi:10.1038/20859, data archived at the World Data Center for Paleoclimatology, Boulder, Colorado, USA., 1999. 4151, 4156, 4187

Porter, S. C.: Some geological implications of average Quaternary glacial conditions, Quaternary Res., 32, 245–261, doi:10.1016/0033-5894(89)90092-6, 1989. 4163

TCD
9, 4147–4203, 2015

Porter, S. C. and Swanson, T. W.: Radiocarbon age constraints on rates of advance and retreat of the Puget Lobe of the Cordilleran Ice Sheet during the last glaciation, Quaternary Res., 50, 205–213, doi:10.1006/qres.1998.2004, 1998. 4149, 4159, 4160, 4163, 4167

Praetorius, S. K. and Mix, A. C.: Synchronization of North Pacific and Greenland climates preceded abrupt deglacial warming, Sience, 345, 444–448, doi:10.1126/science.1252000, 2014. 4150

Prest, V. K., Grant, D. R., and Rampton, V. N.: Glacial map of Canada, "A" Series Map 1253A, Geol. Surv. of Can., Ottawa, ON, doi:10.4095/108979, 1968. 4149, 4170, 4171

Robert, B. L.: Modeling the Cordilleran ice sheet, Geogr. Phys. Quatern., 45, 287–299, doi:10.7202/032876ar, 1991. 4151

Rutter, N., Coronato, A., Helmens, K., Rabassa, J., and Zárate, M.: Glaciations in North and South America from the Miocene to the Last Glacial Maximum: Comparisons, Linkages and Uncertainties, Springer Briefs in Earth System Sciences, Springer, Dordrecht, doi:10.1007/978-94-007-4399-1, 2012. 4149

Ryder, J. M., Fulton, R. J., and Clague, J. J.: The Cordilleran ice sheet and the glacial geomorphology of southern and central British Colombia, Geogr. Phys. Quatern., 45, 365–377, doi:10.7202/032882ar, 1991. 4161

Seguinot, J.: Spatial and seasonal effects of temperature variability in a positive degree-day glacier surface mass-balance model, J. Glaciol., 59, 1202–1204, doi:10.3189/2013JoG13J081, 2013. 4155

Seguinot, J., Khroulev, C., Rogozhina, I., Stroeven, A. P., and Zhang, Q.: The effect of climate forcing on numerical simulations of the Cordilleran ice sheet at the Last Glacial Maximum, The Cryosphere, 8, 1087–1103, doi:10.5194/tc-8-1087-2014, 2014. 4151, 4156, 4162, 4171

Shea, J. M., Moore, R. D., and Stahl, K.: Derivation of melt factors from glacier mass-balance records in western Canada, J. Glaciol., 55, 123–130, doi:10.3189/002214309788608886, 2009. 4155

Sissons, J. B.: The Loch Lomond Stadial in the British Isles, Nature, 280, 199–203, doi:10.1038/280199a0, 1979. 4150

Stea, R. R., Seaman, A. A., Pronk, T., Parkhill, M. A., Allard, S., and Utting, D.: The Appalachian Glacier Complex in Maritime Canada, in: Dev. Quaternary Sci., vol. 15, edited by: Ehlers, J., Gibbard, P. L., and Hughes, P. D., Elsevier, Amsterdam, 631–659, doi:10.1016/b978-0-444-53447-7.00048-9, 2011. 4150

TCD
9, 4147–4203, 2015

Stroeven, A. P., Fabel, D., Codilean, A. T., Kleman, J., Clague, J. J., Miguens-Rodriguez, M., and Xu, S.: Investigating the glacial history of the northern sector of the Cordilleran ice sheet with cosmogenic ^{10}Be concentrations in quartz, Quaternary Sci. Rev., 29, 3630–3643, doi:10.1016/j.quascirev.2010.07.010, 2010. 4149, 4159, 4160, 4163, 4166, 4168

Stroeven, A. P., Fabel, D., Margold, M., Clague, J. J., and Xu, S.: Investigating absolute chronologies of glacial advances in the NW sector of the Cordilleran ice sheet with terrestrial in situ cosmogenic nuclides, Quaternary Sci. Rev., 92, 429–443, doi:10.1016/j.quascirev.2013.09.026, 2014. 4149, 4159, 4160, 4163, 4168

Stroeven, A. P., Hättestrand, C., Kleman, J., Heyman, J., Fabel, D., Fredin, O., Goodfellow, B. W., Harbor, J. M., Jansen, J. D., Olsen, L., Caffee, M. W., Fink, D., Lundqvist, J., Rosqvist, G. C., Strömberg, B., and Jansson, K. N.: Deglaciation of Fennoscandia, Quaternary Sci. Rev., in review, 2015. 4150

Stumpf, A. J., Broster, B. E., and Levson, V. M.: Multiphase flow of the late Wisconsinan Cordilleran ice sheet in western Canada, Geol. Soc. Am. Bull., 112, 1850–1863, doi:10.1130/0016-7606(2000)112<1850:mfotlw>2.0.co;2, 2000. 4161

Taylor, M., Hendy, I., and Pak, D.: Deglacial ocean warming and marine margin retreat of the Cordilleran Ice Sheet in the North Pacific Ocean, Earth Planet. Sc. Lett., 403, 89–98, doi:10.1016/j.epsl.2014.06.026, 2014. 4160, 4168

the PISM authors: PISM, a Parallel Ice Sheet Model, available at: http://www.pism-docs.org (last access: 2015), 2015. 4150, 4152, 4153

Troost, K. G.: The penultimate glaciation and mid-to late-pleistocene stratigraphy in the Central Puget Lowland, Washington, in: 2014 GSA Annual Meeting, Vancouver, 19–22 October 2014, abstract no. 138-9, 2014. 4149, 4159, 4163

Tulaczyk, S., Kamb, W. B., and Engelhardt, H. F.: Basal mechanics of Ice Stream B, west Antarctica: 1. Till mechanics, J. Geophys. Res., 105, 463, doi:10.1029/1999jb900329, 2000. 4154

Turner, D. G., Ward, B. C., Bond, J. D., Jensen, B. J., Froese, D. G., Telka, A. M., Zazula, G. D., and Bigelow, N. H.: Middle to Late Pleistocene ice extents, tephrochronology and paleoenvironments of the White River area, southwest Yukon, Quaternary Res., 75, 59–77, doi:10.1016/j.quascirev.2013.05.011, 2013. 4149

Ward, B. C., Bond, J. D., and Gosse, J. C.: Evidence for a 55–50 ka (early Wisconsin) glaciation of the Cordilleran ice sheet, Yukon Territory, Canada, Quaternary Res., 68, 141–150, doi:10.1016/j.yqres.2007.04.002, 2007. 4149, 4159

TCD
9, 4147–4203, 2015

Ward, B. C., Bond, J. D., Froese, D., and Jensen, B.: Old Crow tephra (140 ± 10 ka) constrains penultimate Reid glaciation in central Yukon Territory, Quaternary Res., 27, 1909–1915, doi:10.1016/j.quascirev.2008.07.012, 2008. 4149, 4166

Winkelmann, R., Martin, M. A., Haseloff, M., Albrecht, T., Bueler, E., Khroulev, C., and Levermann, A.: The Potsdam Parallel Ice Sheet Model (PISM-PIK) – Part 1: Model description, The Cryosphere, 5, 715–726, doi:10.5194/tc-5-715-2011, 2011. 4153, 4154

TCD
9, 4147–4203, 2015

Table 1. Parameter values used in the ice sheet model.

Not.	Name	Value	Unit
ρ	Ice density	910	$\mathrm{kg\,m^{-3}}$
g	Standard gravity	9.81	$\mathrm{m\,s^{-2}}$
Basal sliding			
q	Pseudo-plastic sliding exponent	0.25	–
v_{th}	Pseudo-plastic threshold velocity	100.0	$\mathrm{m\,yr^{-1}}$
c_0	Till cohesion	0.0	Pa
δ	Effective pressure coefficient	0.02	–
e_0	Till reference void ratio	0.69	–
C_{c}	Till compressibility coefficient	0.12	–
W_{max}	Maximal till water thickness	2.0	m
Bedrock and lithosphere			
ρ_{b}	Bedrock density	3300	$\mathrm{kg\,m^{-3}}$
c_{b}	Bedrock specific heat capacity	1000	$\mathrm{J\,kg^{-1}\,K^{-1}}$
k_{b}	Bedrock thermal conductivity	3.0	$\mathrm{J\,m^{-1}\,K^{-1}\,s^{-1}}$
v_m	Astenosphere viscosity	1×10^{19}	Pa s
ρ_l	Lithosphere density	3300	$\mathrm{kg\,m^{-3}}$
D	Lithosphere flexural rigidity	5.0×10^{24}	N
Surface and atmosphere			
T_{s}	Temperature of snow precipitation	273.15	K
T_{r}	Temperature of rain precipitation	275.15	K
F_{s}	Degree-day factor for snow	3.04×10^{-3}	$\mathrm{m\,K^{-1}\,day^{-1}}$
F_{i}	Degree-day factor for ice	4.59×10^{-3}	$\mathrm{m\,K^{-1}\,day^{-1}}$
γ	Air temperature lapse rate	6×10^{-3}	$\mathrm{K\,m^{-1}}$

TCD
9, 4147–4203, 2015

Table 2. Palaeo-temperature proxy records and scaling parameters yielding temperature offset time-series used to force the ice sheet model through the last glacial cycle (Fig. 3). f corresponds to the scaling factor adopted to yield last glacial maximum ice limits in the vicinity of mapped end moraines, and $T_{[32,22]}$ refers to the resulting mean temperature anomaly during the period −32 to −22 ka after scaling.

Record	Latitude	Longitude	Elev. (m a.s.l.)	Proxy	f	$T_{[32,22]}$ (K)	Reference
GRIP	72°35′ N	37°38′ W	3238	δ^{18}O	0.37	−5.8	Dansgaard et al. (1993)
NGRIP	75°06′ N	42°19′ W	2917	δ^{18}O	0.24	−6.5	Andersen et al. (2004)
EPICA	75°06′ S	123°21′ E	3233	δ^{18}O	0.64	−5.9	Jouzel et al. (2007)
Vostok	78°28′ S	106°50′ E	3488	δ^{18}O	0.74	−5.9	Petit et al. (1999)
ODP 1012	32°17′ N	118°23′ W	−1772	$U^{K'}_{37}$	1.61	−6.1	Herbert et al. (2001)
ODP 1020	41°00′ N	126°26′ W	−3038	$U^{K'}_{37}$	1.20	−6.0	Herbert et al. (2001)

TCD
9, 4147–4203, 2015

Table 3. Extremes in Cordilleran ice sheet volume and extent corresponding to MIS 4, 3 and 2 for each of the six low-resolution simulations (Fig. 3).

Record	Age (ka)			Ice extent (10^6 km^2)			Ice volume (m s.l.e.)		
	MIS 4	MIS 3	MIS 2	MIS 4	MIS 3	MIS 2	MIS 4	MIS 3	MIS 2
GRIP	57.45	42.93	19.14	1.87	0.69	2.07	7.35	1.69	8.71
NGRIP	60.25	45.86	22.85	2.11	0.74	2.10	8.84	1.82	8.76
EPICA	61.89	45.30	17.23	1.51	1.01	2.09	5.11	2.74	8.91
Vostok	60.86	41.25	16.84	1.51	1.03	2.01	5.15	2.88	8.40
ODP 1012	56.46	47.39	23.19	1.38	0.90	2.07	4.39	2.35	8.62
ODP 1020	60.23	52.97	20.56	1.25	0.72	2.09	3.84	1.75	8.81
Minimum	61.89	52.97	23.19	1.25	0.69	2.01	3.84	1.69	8.40
Maximum	56.46	41.25	16.84	2.11	1.03	2.10	8.84	2.88	8.91

TCD
9, 4147–4203, 2015

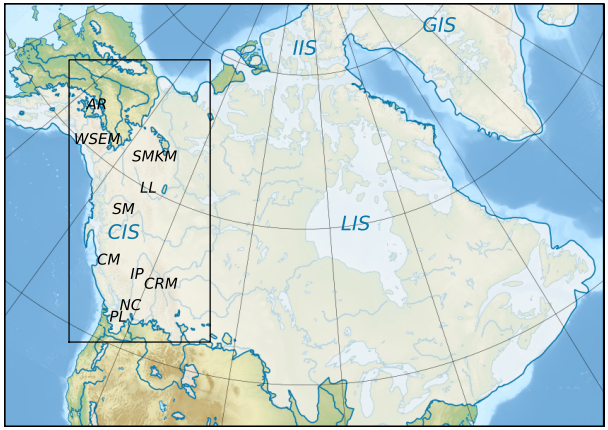

Figure 1. Relief map of northern North America showing a reconstruction of the areas once covered by the Cordilleran (CIS), Laurentide (LIS), Innuitian (IIS), and Greenland (GIS) ice sheets during the last 18 ^{14}C ka (21.4 cal ka, Dyke, 2004). The rectangular box denotes the location of the modelling domain used in this study. Major mountain ranges covered by the ice sheet include the Alaska Range (AR), the Wrangell and Saint Elias mountains (WSEM), the Selwyn and Mackenzie mountains (SMKM), the Skeena Mountains (SM), the Coast Mountains (CM), the Columbia and Rocky Mountains (CRM), and the North Cascades (NC). Major depressions include the Liard Lowland (LL), the Interior Plateau of British Columbia (IP), and the Puget Lowland (PL). The background map consists of ETOPO1 (Amante and Eakins, 2009) and Natural Earth Data (Patterson and Kelso, 2015).

TCD
9, 4147–4203, 2015

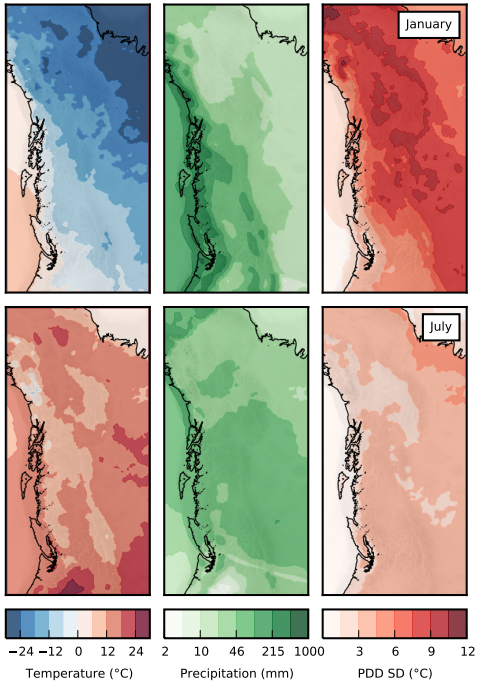

Figure 2. Monthly mean near-surface air temperature, precipitation, and standard deviation of daily mean temperature (PDD SD) for January and July from the North American Regional Reanalysis (NARR; Mesinger et al., 2006), used to force the surface mass balance (PDD) component of the ice sheet model. Note the strong contrasts in seasonality, timing of the precipitation peak, and temperature variability over the model domain, notably between coastal and inland regions.

TCD
9, 4147–4203, 2015

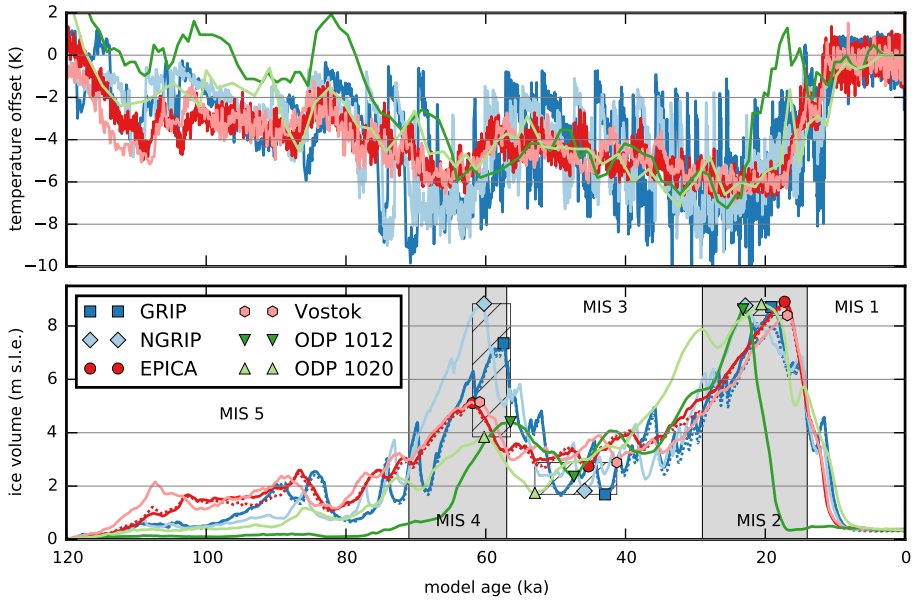

Figure 3. Temperature offset time-series from ice core and ocean records (Table 2) used as palaeo-climate forcing for the ice sheet model (top panel), and modelled ice volume (bottom panel) through the last 120 ka. Ice volumes are expressed in meters of sea level equivalent (m s.l.e.). Gray fields indicate Marine Oxygen Isotope Stage (MIS) boundaries for MIS 2 and MIS 4 according to a global compilation of benthic δ^{18}O records (Lisiecki and Raymo, 2005). Hatched rectangles highlight the time-volume span for ice volume extremes corresponding to MIS 4 (61.9–56.5 ka), MIS 3 (53.0–41.3 ka), and MIS 2 (LGM, 23.2–16.8 ka). Dotted lines correspond to GRIP- and EPICA-driven 5 km-resolution runs.

TCD
9, 4147–4203, 2015

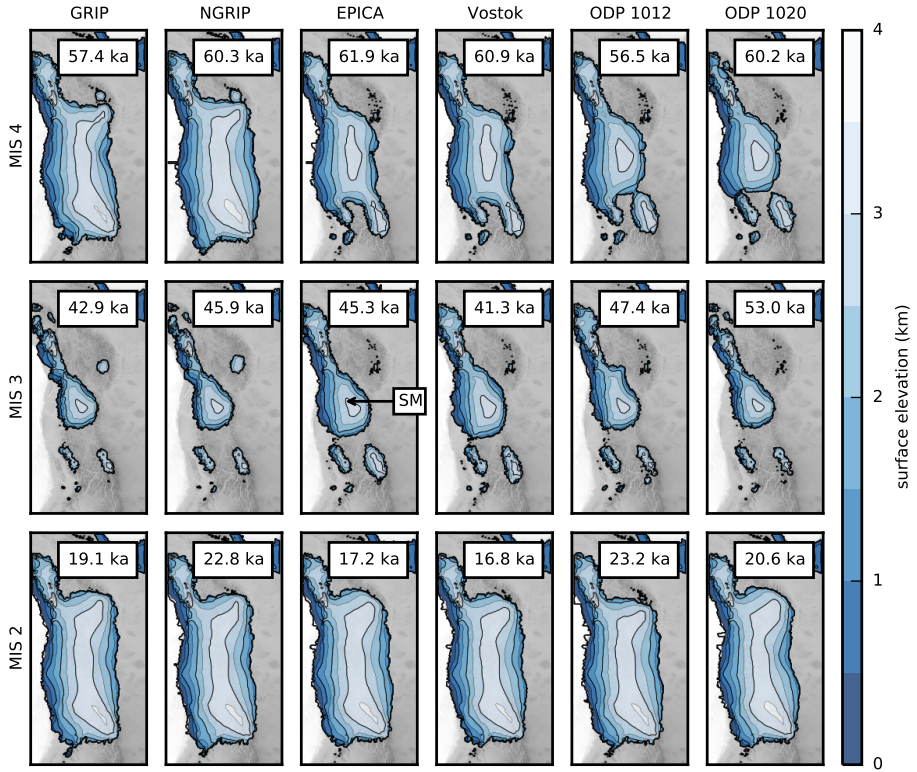

Figure 4. Snapshots of modelled surface topography (500 m contours) corresponding to the ice volume extremes indicated on Fig. 3. An ice cap persists over the Skeena Mountains (SM) during MIS 3. Note the occurence of spatial similarities despite large differences in timing.

TCD
9, 4147–4203, 2015

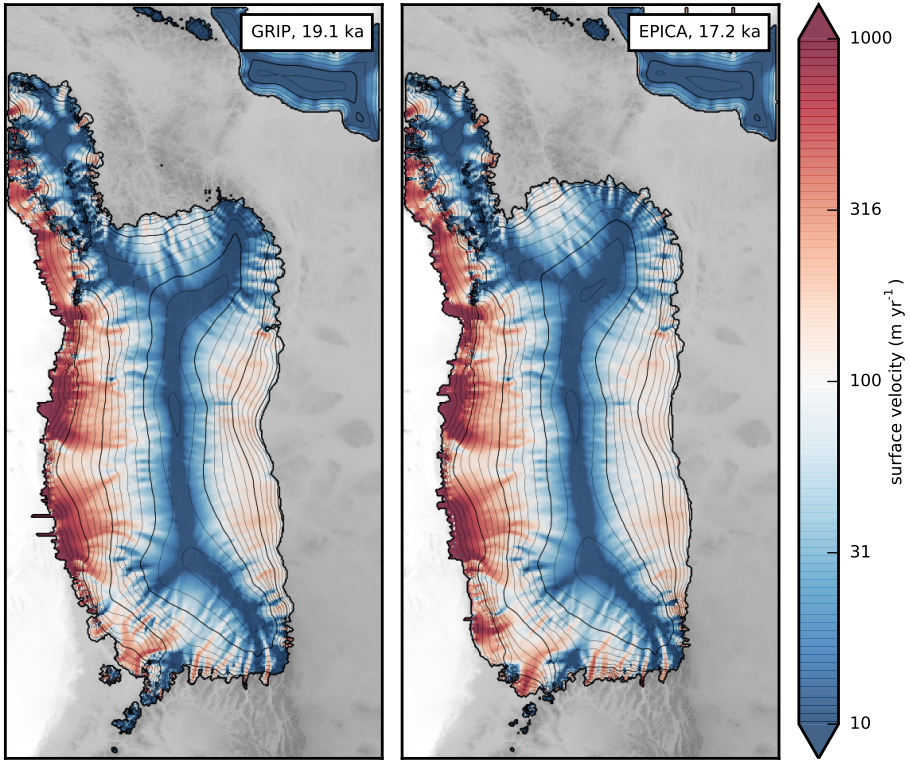

Figure 5. Modelled surface topography (200 m contours) and surface velocity (colour mapping) corresponding to the maximum ice volume during MIS 2 in the GRIP and EPICA high-resolution simulations.

TCD
9, 4147–4203, 2015

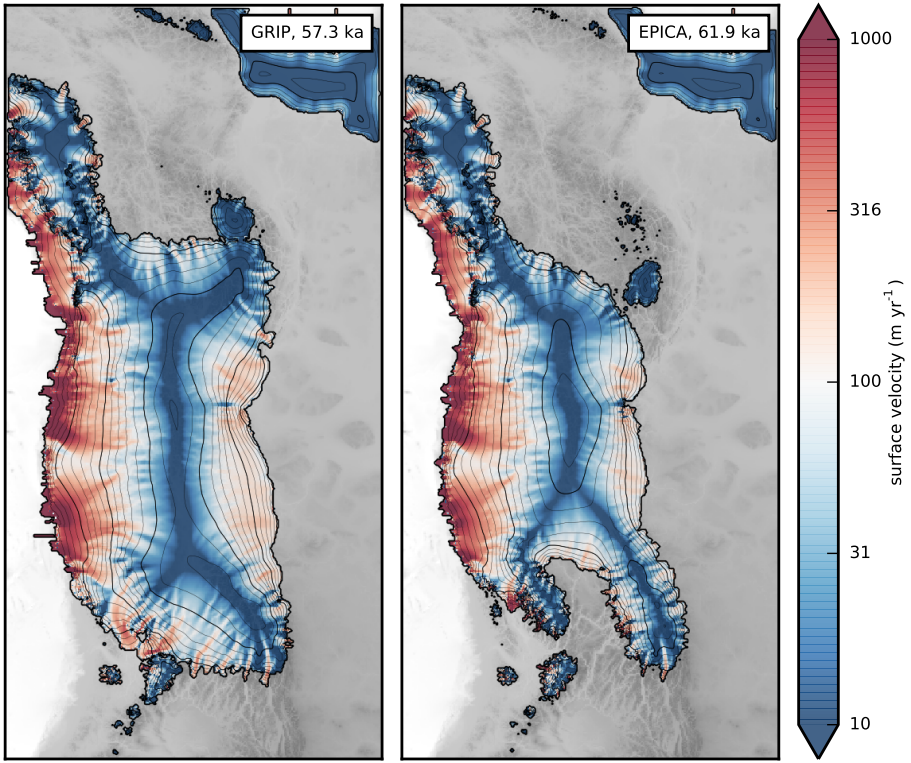

Figure 6. Modelled surface topography (200 m contours) and surface velocity (colour mapping) corresponding to the maximum ice volume during MIS 4 in the GRIP and EPICA high-resolution simulations.

TCD
9, 4147–4203, 2015

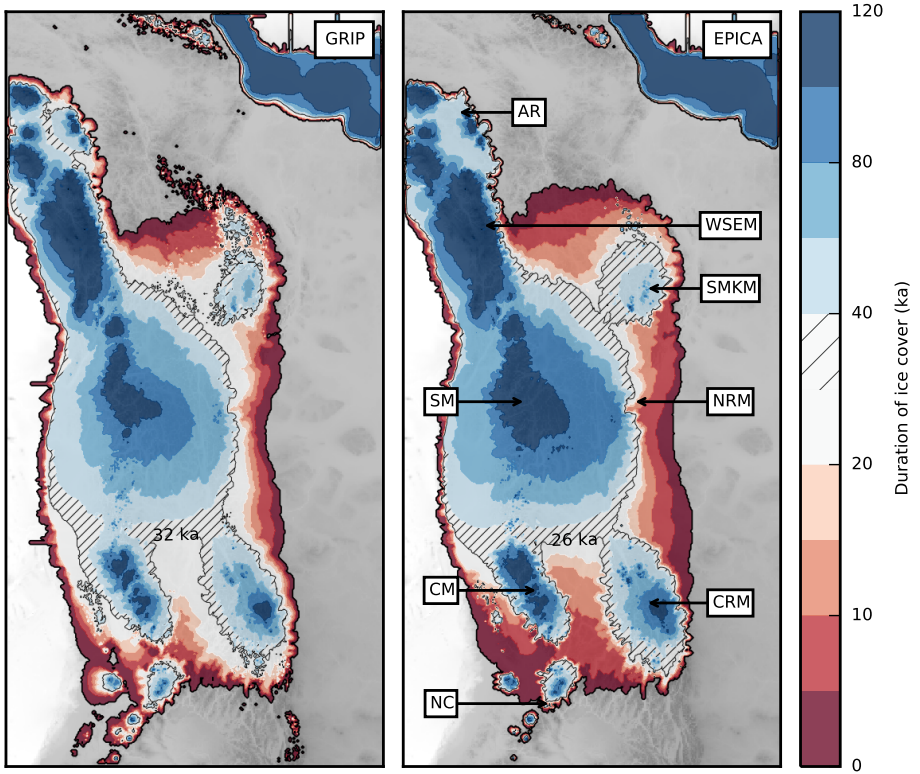

Figure 7. Modelled duration of ice cover during the last 120 ka using GRIP and EPICA climate forcing. Note the irregular colour scale. A continuous ice cover spanning from the Alaska Range (AR) to the Coast Mountains (CM) and the Columbia and Rocky mountains (CRM) exists for about 32 ka in the GRIP simulation and 26 ka in the EPICA simulation. The maximum extent of the ice sheet generally corresponds to relatively short durations of ice cover, but ice cover persists over the Skeena Mountains (SM) during most of the simulation. See Fig. 1 for a list of abbreviations.

TCD
9, 4147–4203, 2015

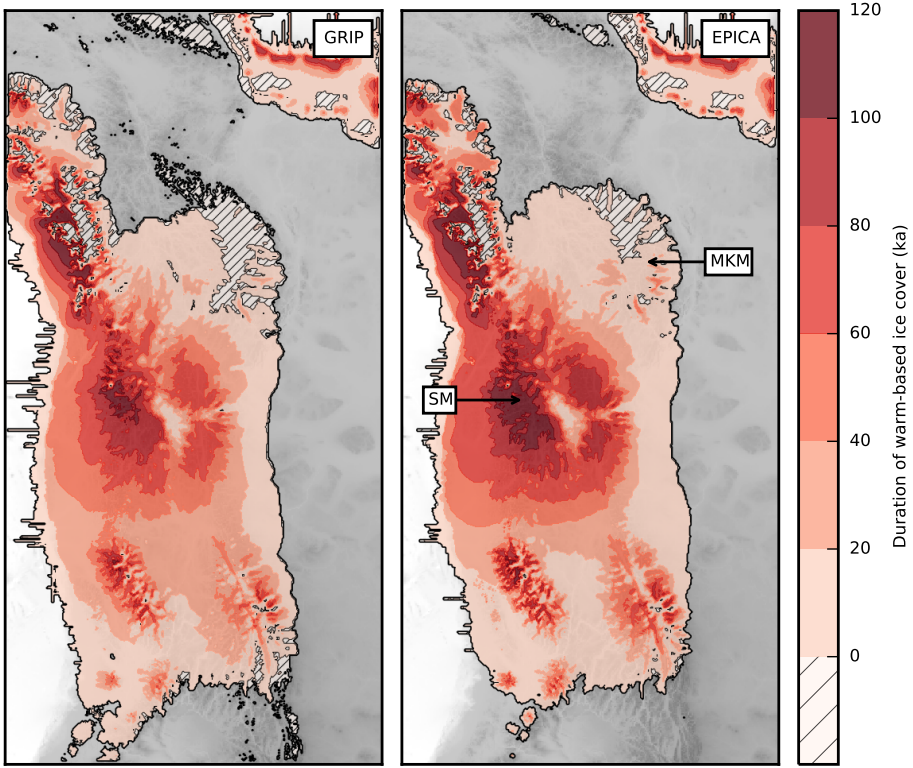

Figure 8. Modelled duration of warm-based ice cover during the last 120 ka. Long ice cover durations combined with basal temperatures at the pressure melting point may explain the strong glacial erosional imprint of the Skeena Mountains (SM) landscape. Hatches indicate areas that were covered by cold ice only.

TCD
9, 4147–4203, 2015

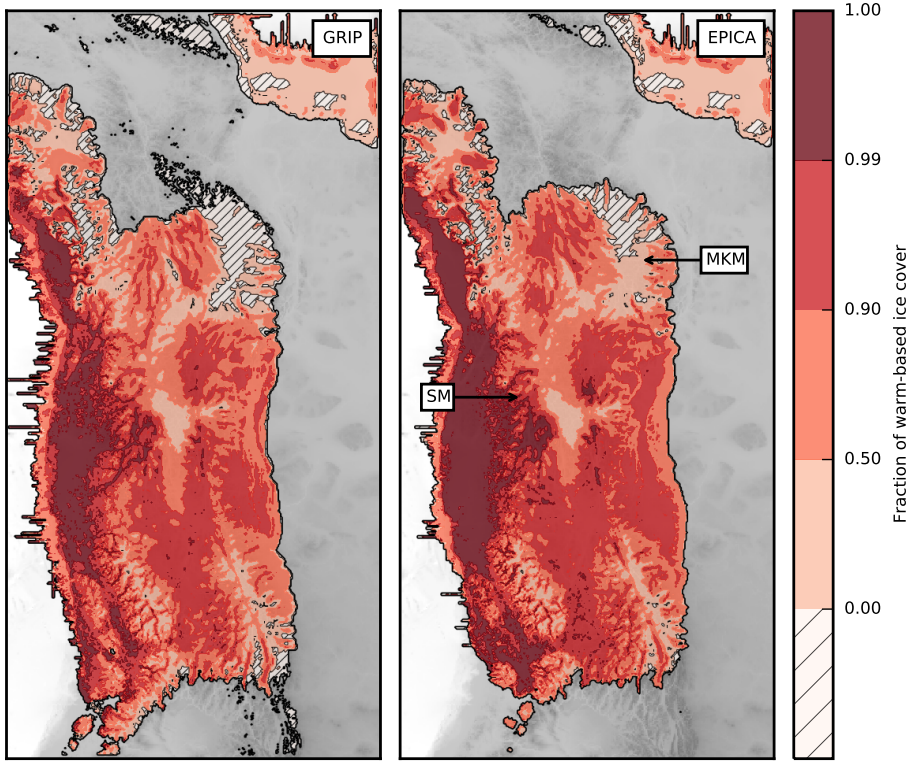

Figure 9. Modelled fraction of warm-based ice cover during the ice-covered period. Note the dominance of warm-based conditions on the continental shelf and major glacial troughs of the coastal ranges. Hatches indicate areas that were covered by cold ice only.

TCD
9, 4147–4203, 2015

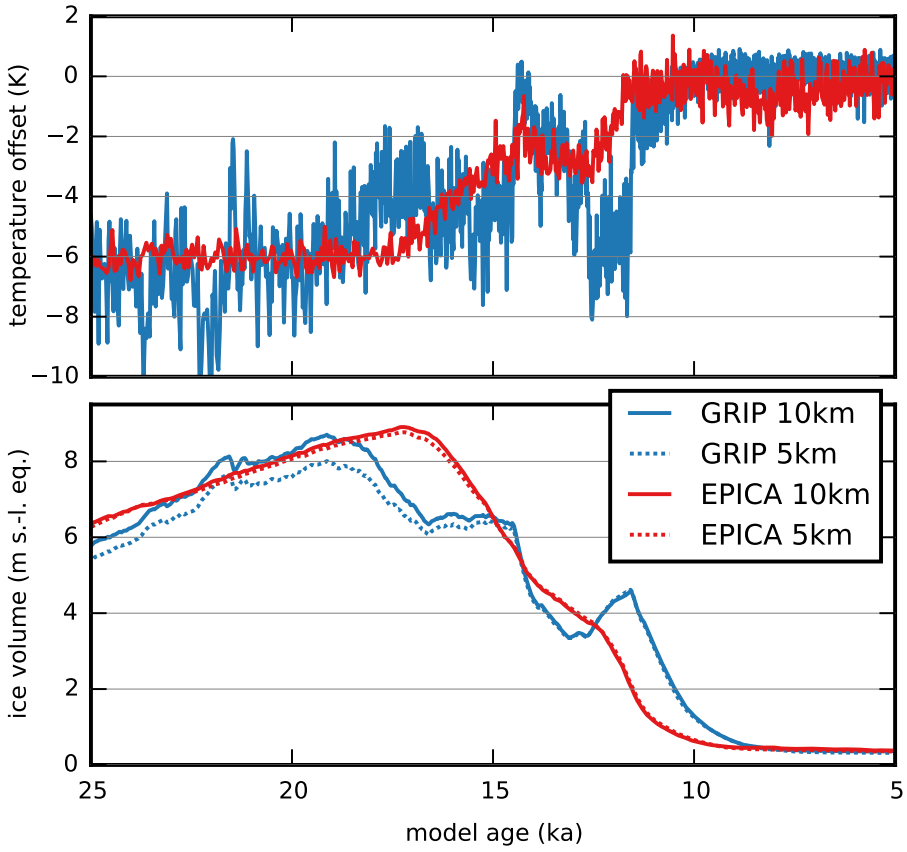

Figure 10. Temperature offset time-series from the GRIP and EPICA ice core records (Table 2) (top panel), and modelled ice volume during the deglaciation, expressed in meters of sea-level equivalent (bottom panel).

TCD
9, 4147–4203, 2015

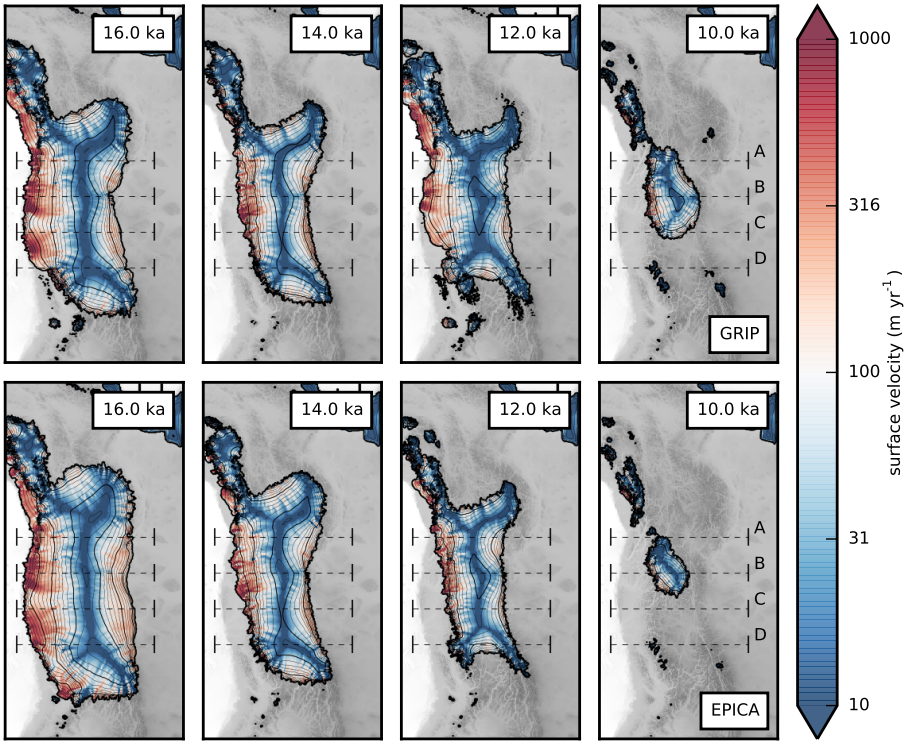

Figure 11. Snapshots of modelled surface topography (200 m contours) and surface velocity (colour mapping) during the last deglaciation from the GRIP (top panels) and EPICA (bottom panels) 5 km simulations. Dashed segments **(A–D)** indicate the location of profiles used in Figs. 14 and 15.

TCD
9, 4147–4203, 2015

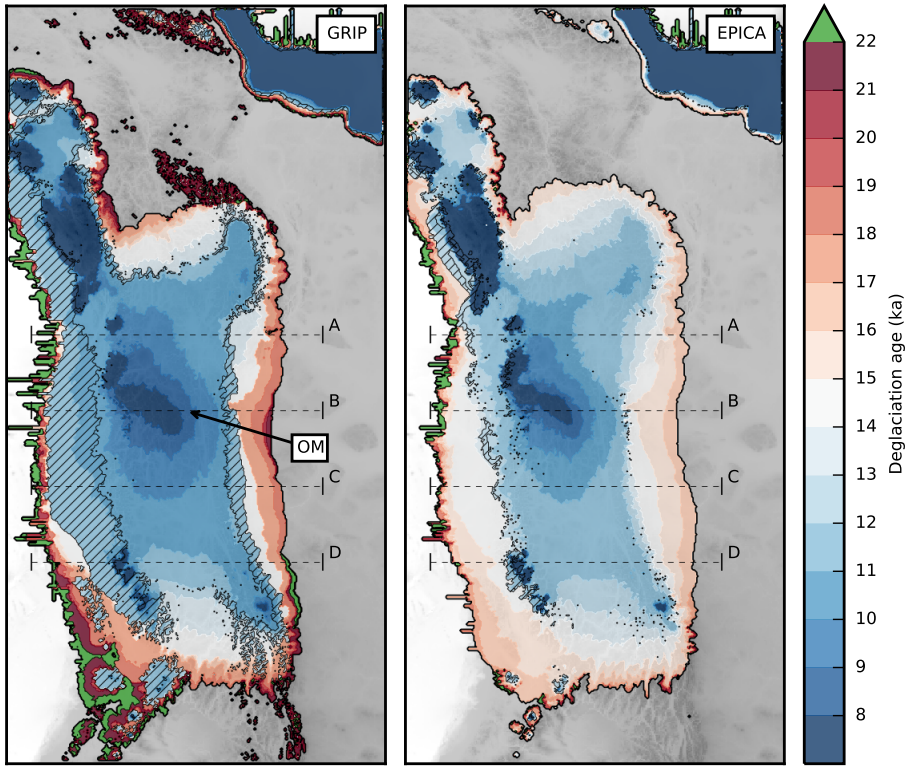

Figure 12. Modelled age of the last deglaciation. Areas that have been covered only before the last glacial maximum are marked in green. Hatches denote re-advance of mountain-centred ice caps and the decaying ice sheet between 14 and 10 ka. Dashed segments **(A–D)** indicate the location of profiles used in Figs. 14 and 15.

TCD
9, 4147–4203, 2015

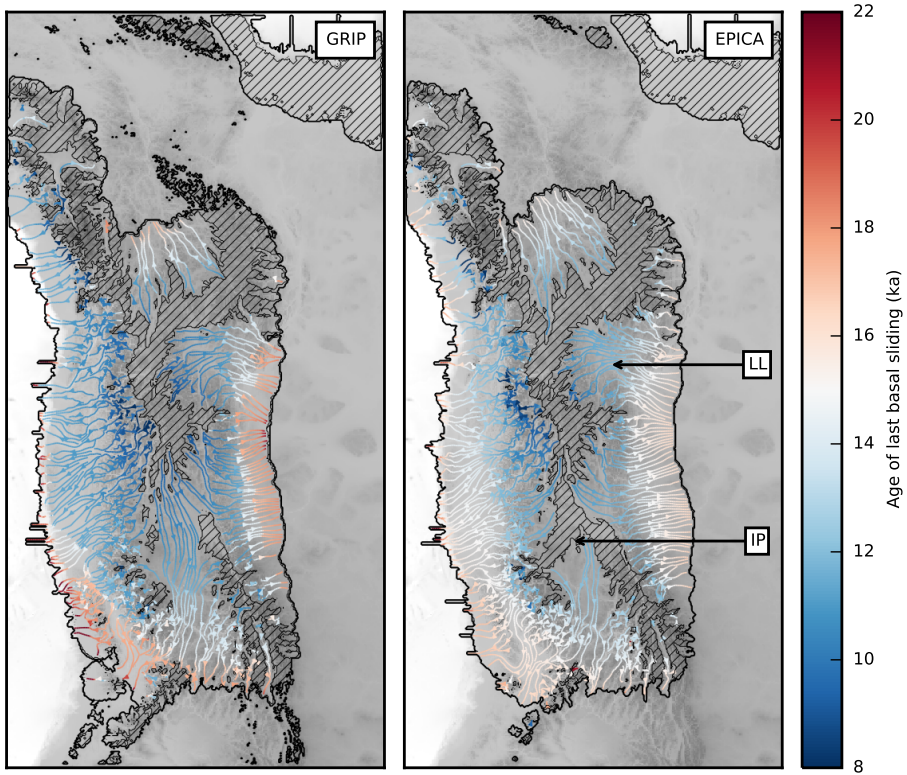

Figure 13. Modelled deglacial basal ice velocities. Hatches indicate areas that remain non-sliding throughout deglaciation (22.0–8.0 ka), notably including parts of the Interior Plateau (IP). Note the concentric patterns of deglacial flow in the Liard Lowland (LL). Sliding grid cells were distinguished from non-sliding grid cells using a basal velocity threshold of 1 m yr^{-1}.

TCD
9, 4147–4203, 2015

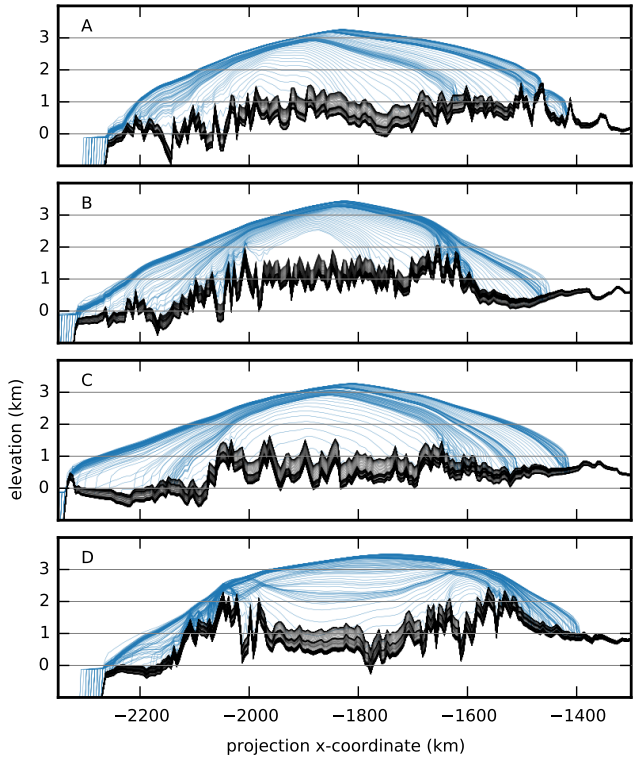

Figure 14. Modelled bedrock (black) and ice surface (blue) topography profiles during deglaciation (22.0–8.0 ka) in the GRIP 5 km simulation, corresponding to the four transects indicated in Figs. 11 and 12.

TCD
9, 4147–4203, 2015

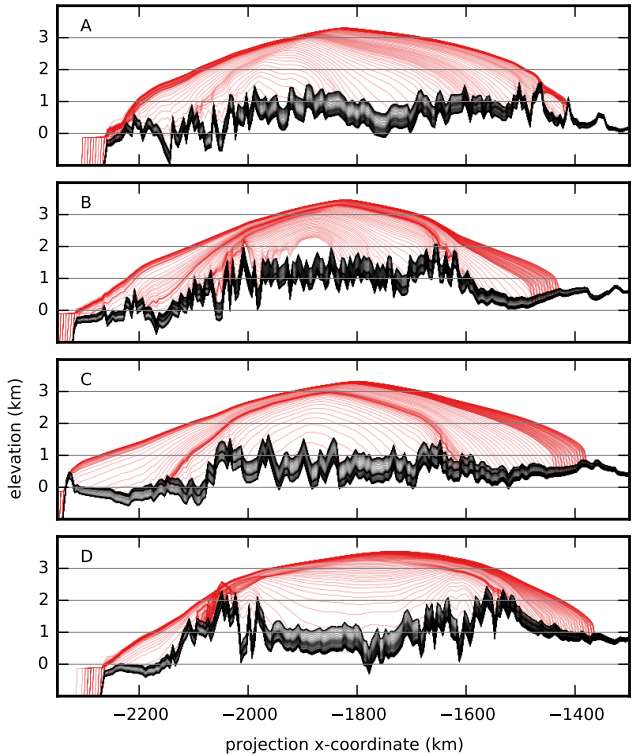

Figure 15. Modelled bedrock (black) and ice surface (red) topography profiles during deglaciation (22.0–8.0 ka) in the EPICA 5 km simulation, corresponding to the four transects indicated in Figs. 11 and 12.

TCD
9, 4147–4203, 2015